Chemical Research in Toxicology

ARTICLE

pubs.acs.org/crt

Fluorescent Properties and Conformational Preferences of C-Linked Phenolic-DNA Adducts

Alireza Omumi,[†,§] Andrea L. Millen,[‡,§] Stacey D. Wetmore,[*,‡] and Richard A. Manderville[*,†]

[†]Departments of Chemistry and Toxicology, University of Guelph, Guelph, ON, Canada N1G 2W1

[‡]Department of Chemistry & Biochemistry, University of Lethbridge, Lethbridge, AB, Canada T1K 3M4

Supporting Information

ABSTRACT: Phenolic toxins and mutagenic diazoquinones generate C-linked adducts at the C8 site of 2′-deoxyguanosine (dG) through the intermediacy of radical species. We have previously reported the site-specific incorporation of these adducts into oligonucleotides using a postsynthetic palladium-catalyzed cross-coupling strategy [Omumi et al. (2011) J. Am. Chem. Soc. 133, 42−50]. We report here the structural impact of these lesions within two decanucleotide sequences containing either 5′- and 3′-flanking pyrimidines or purines. In the complementary strands, the base opposite (N) the C-linked adduct was varied to determine the possibility of mismatch stabilization by the modified nucleobases. The resulting adducted duplex structures were characterized using UV thermal denaturation studies, circular dichroism, fluorescence spectroscopy, and molecular dynamics (MD) simulations. The experimental data showed the C-linked adducts to destabilize the duplex when base paired with its normal partner C but to increase duplex stability within a G:G mismatch. The stabilization within the G:G mismatch was sequence dependent, with flanking purine bases playing a key role in the stabilizing influence of the adduct. MD simulations showed no large structural changes to the B form double helix, regardless of the (*anti*/*syn*) adduct preference. Consideration of H-bonding and stacking interactions derived from the MD simulations together with the thermal melting data and changes in fluorescent emission of the adducts upon hybridization to the complementary strands implied that the C-linked phenolic adducts preferentially adopt the *syn*-conformation within both duplexes regardless of the opposite base N. Given that biological outcome in terms of mutagenicity appears to be strongly correlated to the conformational preference of the corresponding N-linked C8-dG adducts, the potential biological implications of phenolic C-linked adducts are discussed.

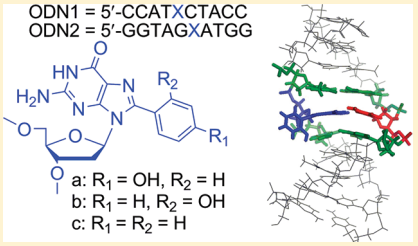

INTRODUCTION

Phenols are ubiquitous substances that exhibit both antioxidant and pro-oxidant properties. Vitamin E[1] and polyphenols[2] are beneficial antioxidants, while chlorophenols[3] are deleterious pro-oxidants. Interestingly, both activities can stem from oxidation of the parent phenol to generate a phenoxyl radical.[4] Vitamin E and polyphenols quench reactive oxygen species (ROS), such as hydroxyl radical (HO•), to generate relatively stable phenoxyl radicals.[1,2] Electron-withdrawing chlorine substituents decrease phenoxyl radical stability,[5] leading to oxidative stress in biological systems.[6]

Phenoxyl radicals can also react with the nucleobases to afford bulky DNA adducts.[7−10] Structural evidence shows a tendency for attachment at the C8 position of 2′-deoxyguanosine (dG), as noted with HO• in the formation of 8-oxo-dG.[11] The phenoxyl radicals also display ambident [oxygen (O) vs carbon (C)] electrophilicity in reactions with dG, as outlined in Scheme 1.[12,13] Oxidation of pentachlorophenol (PCP) with peroxidase enzymes generates an O-linked adduct,[7,8] while metabolism of the chlorophenolic mycotoxin ochratoxin A favors C-linked adduct formation.[9,10] The specific C-linked adducts shown in Scheme 1 are also generated by mutagenic diazoquinones[14] and are structurally related to a family of 8-aryl(Ar)-dG adducts produced by aryl hydrazines,[15−17] polycyclic aromatic hydrocarbons (PAHs),[18] estrogens,[19] and nitroaromatics.[20] Given the importance of N-linked adducts in arylamine carcinogenesis,[21−23] O-linked and C-linked adducts are expected to play a role in phenol toxicity.

To study the properties of DNA adducts, synthetic methods for their preparation and insertion into oligonucleotides are critical. For N-linked adducts, Pd-catalyzed cross-coupling between arylamine and protected 8-Br-dG can be used to synthesize the nucleoside,[24,25] which is then converted into a phosphoramidite for incorporation into oligonucleotides using solid-phase DNA synthesis.[26−28] Structural studies have shown that C8 attachment of the bulky N-linked arylamine can shift the conformational equilibrium of the glycosidic bond from *anti* to *syn*, leading to distinct mutation and repair outcomes.[29] For example, the N-linked 8-acetylaminofluorene-G (AAF-G) lesion can adopt three different conformers in duplex DNA.[30] When Watson−Crick base-paired with C, *anti*-AAF-G adopts a non-distorting B type structure.[30] In the *syn*-conformation, a base-displaced intercalated of "stacked" (S) structure is formed in

Received: June 13, 2011
Published: September 09, 2011

ACS Publications © 2011 American Chemical Society

Scheme 1

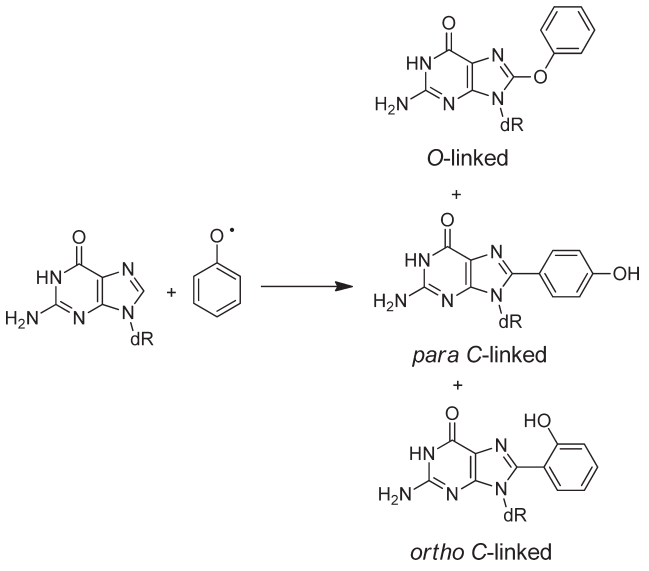

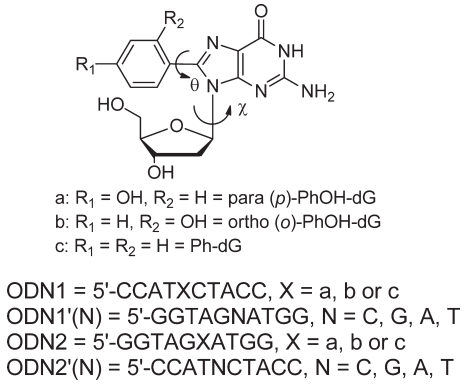

Figure 1. Structures of C-linked nucleoside adducts and oligonucleotide sequences.

which the bulky AAF group intercalates into the helix and displaces C.[30,31] When mismatched with purine bases, a minor groove binding "wedged" (W) structure is formed with *syn*-AAF-G forming a Hoogsteen bonding arrangement with the purine base.[30]

For the C-linked adducts derived from phenolic toxins, we have recently developed a postsynthetic Pd-catalyzed cross-coupling strategy for their insertion into oligonucleotides.[32] This strategy was prompted by our findings that C-linked phenolic adducts are sensitive to acids[33] and oxidants,[34] making solid-phase DNA synthesis problematic,[32] and that they are too bulky to be used as substrates for DNA polymerases,[35] precluding an enzymatic strategy for their synthesis. Purification of the adducted oligonucleotides using HPLC was facilitated by the fluorescent nature of the C-linked phenolic adducts.[36−38] Fluorescent DNA adducts are also sensitive probes for gaining insight into the conformational preference of the adduct within DNA helices.[39,40] Our previous studies[38,41] on the conformations of 8-(4″-hydroxyphenyl)-dG (*p*-PhOH-dG) and 8-(2″-hydroxyphenyl)-dG (*o*-PhOH-dG) (Figure 1) imply that the energy differences between *anti* and *syn* are likely quite small and that both orientations may be present in duplex DNA.[41] The effect of H-bonding interactions on the *anti*/*syn* conformational stability[42] shows that *o*-PhOH-dG forms significantly more stable complexes with the Watson−Crick face than with the Hoogsteen face and that C forms the most stable base pair with *o*-PhOH-dG regardless of the H-bonding face involved. However, for *p*-PhOH-dG, Hoogsteen interactions are stronger than those with natural dG, and the *para*-adduct binds with nearly equal stability to both C and G in the Hoogsteen orientation.[42]

The present work expands our understanding on the conformation and binding preference of C-linked phenolic adducts and considers the structural impact of *p*-PhOH-dG, *o*-PhOH-dG, and 8-phenyl-dG (Ph-dG) within the two decanucleotides oligonucleotide 1 (ODN1) and ODN2 shown in Figure 1. In ODN1, the C-linked adducts (X) are flanked by pyrimidine bases, while in ODN2, they are flanked by purines. In the complementary strands, ODN1′(N), and ODN2′(N), the base opposite (N) the adduct has been varied (N = C, G, A, T) to determine the possibility of mismatch stabilization by the modified C-linked nucleobases. Our work highlights the ability of these lesions to stabilize a G:G mismatch in duplex DNA and represents a first step in understanding the potential biological significance of C-linked phenolic-DNA adducts.

EXPERIMENTAL PROCEDURES

General. ^{1}H and ^{13}C NMR spectra were recorded at room temperature on a Bruker Avance 300 DPX at 300.1 and 75.5 MHz, respectively. NMR spectra were referenced to the solvent signal of the deuterated solvent. Mass spectra were conducted at the Biological Mass Spectrometry Facility (BMSF) at the University of Guelph and were obtained from a Micromass/Waters Global Ultima quadrupole TOF using electrospray ionization. UV−vis and fluorescence emission spectra were recorded on a Cary 300-Bio UV−visible Spectrophotometer and Cary Eclipse Fluorescence Spectrophotometer with built-in Peltier temperature controllers. Standard 10 mm light path quartz glass cells from Hellma GmbH & Co. (Concord, ON) were used for both UV−vis and fluorescence measurements. All UV−vis and fluorescence emission spectra were recorded with baseline correction and stirring. Any water used for buffers or spectroscopic solutions was obtained from a Milli-Q filtration system (18.2 MΩ). pH measurements were taken at room temperature with an Accumet 910 pH meter with an Accumet pH Combination Electrode with stirring.

Unless otherwise noted, commercial compounds were used as received. Arylboronic acids (phenyl, 4-hydroxyphenyl, and 2-hydroxyphenyl) were purchased from Frontier Scientific (Logan, UT), $Pd(OAc)_2$ was from Sigma-Aldrich (Oakville, ON), dG was from ChemGenes (Wilmington, MA), and 3,3′,3″-phosphinidynetris(benzenesulfonic acid) trisodium salt (TPPTS) was from Alfa Aesar (Ward Hill, MA). The synthesis of 8-bromo-2′-deoxyguanosine (8-Br-dG) was performed according to literature procedures by treating dG with *N*-bromosuccinimide in water-acetonitrile.[43] Suzuki−Miyaura cross-coupling reactions of 8-Br-dG with arylboronic acids were conducted according to the literature[44] and NMR, and MS spectra for *p*-PhOH-dG,[37,38] *o*-PhOH-dG,[36,38] and Ph-dG[34,44] were identical to those previously published.

Photophysical Properties. Stock solutions of *p*-PhOH-dG, *o*-PhOH-dG, and Ph-dG were prepared in DMSO (due to sparing solubility in other solvents) to a concentration of 4 mM. Spectroscopic solutions were prepared with 5 μL of stock solution and 1995 μL of either 10 mM MOPS (pH 7.0, μ = 0.1 M NaCl) or $CHCl_3$. UV−vis spectral measurements were observed from 220 to 400 nm, with fluorescence spectra recorded at an excitation wavelength of 290 nm, with emission recorded from 320 to 500 nm. Excitation and emission slit widths were kept constant at 2.5 nm.

Quantum Yield Measurement. The quantum yield value for Ph-dG was determined in 10 mM MOPS buffer (pH 7.0, μ = 0.1 M NaCl) using the comparative method.[45] Quinine bisulfate (ϕ_{fl} = 0.546) in 0.5 M H_2SO_4 was used as the fluorescence quantum yield standard.[46] The following equation was used to calculate fluorescence quantum yields:

$$\phi_{fl}(x) = (A_s/A_x)(F_x/F_s)(\eta_x/\eta_s)_2\phi_{fl}(s)$$

where s is the standard, x is the unknown, A is the absorbance at the excitation wavelength, F is the integrated area under the emission curve, η is the refractive index of the solvent, and ϕ_{fl} is the quantum yield. The refractive index corrective term was not included due to the similar refractive indices of H_2O and 0.5 M H_2SO_4. Excitation and emission slit widths were kept constant for all fluorescence measurements at 2.5 nm. Absorbance readings were kept below 0.06 to avoid inner-filter and self-absorbance phenomena.

Cyclic Voltammetry (CV). Electrochemical oxidation measurements for *o*-PhOH-dG and Ph-dG were conducted in a three-electrode glass cell under nitrogen. Measurements were carried out in a solution of 0.1 M *N*,*N*-dimethylformamide (DMF)/tetrabutylammonium hexafluorophosphate (TBAF). The working electrode used was glassy carbon, 2 mm in diameter. The electrode was polished and ultrasonically rinsed with ethanol. A silver wire placed in a 0.1 M DMF/TBAF solution was used as the reference electrode and was separated from the main solution by a fine porosity frit. The reference electrode potential was calibrated in situ against 1 mol equiv of 9,10-anthraquinone (−0.800 V vs SCE). The counter electrode used was platinum wrapped in foil. For all CVs, the starting potential was 0 V, and the potential was first scanned 1.8 V toward positive potentials and then scanned 1.8 V toward negative potentials. The scanning rate used was 0.2 V/s. Peak picking was achieved by correlation of values obtained from automatic software methods and manual assignment.

Suzuki−Miyaura Coupling Reactions of Arylboronic Acids with 8-Br-G-Modified Oligonucleotides. The oligonucleotide substrates containing 8-Br-dG for the synthesis of ODN1_a,b,c and ODN2_a,b,c were custom-made by Sigma Genosys (Oakville, ON) in 1 μmol scale using standard phosphoramidites and 8-Br-dG-CE phosphoramidite purchased from Glen Research (Sterling, VA). Oligonucleotides were cleaved from the solid support and deprotected in ammonium hydroxide at room temperature (to lessen debromination) for 24 h. For Suzuki−Miyaura coupling of arylboronic acids with the brominated oligonucleotides (Br-DNA) (0.1 μmol), the conditions outlined previously were employed.[32] The resulting adducted oligonucleotides were purified by HPLC using an Agilent 1200 series HPLC equipped with an autosampler, autocollector, diode array detector (monitored at 258 and 280 nm), and fluorescence detector (λ_{ext} = 280 nm; λ_{em} = 390 nm). Separation was carried out using a Phenomenox (Torrance, CA) Clarity 3 μ Oligo-RP C18 column (50 mm × 4.60 mm, 3 μ) and various gradients of buffer B in buffer A, in which buffer A was aqueous 50 mM triethylammonium acetate (TEAA), pH 7.2:acetonitrile (95:5) and buffer B was aqueous 50 mM TEAA, pH 7.2:acetonitrile (25:75). Yields (ODN1_a = 79%, ODN1_b = 83%, ODN1_c = 55%, ODN2_a = 77%, ODN2_b = 83%, and ODN2_c = 97%) were estimated by quantification of the isolated product by UV using ε_{260} (nearest neighbor method) for the unmodified oligonucleotides, 87700 cm^{-1} M^{-1} for unmodified ODN1 and 106000 cm^{-1} M^{-1} for unmodified ODN2 (i.e., X = G).

MS Spectra of Oligonucleotides. Modified oligonucleotides ODN1_a,b,c and ODN2_a,b,c were dissolved in 50% water in methanol with 0.1 mM ammonium acetate for mass spectral analysis. Full scan mass spectra were acquired by infusion through an electrospray ionization source in negative mode (ESI^-) using a Waters Q-TOF Micro quadrupole time-of-flight instrument. Low voltages were used for the cone (14 V) and extraction cone (1 V) for oligonucleotide detection. ESI^- MS ODN1_a (m/z) calcd, 3039.6; observed $[M - 3H]^{3-}$ = 1012.2; found, 3039.6. ODN1_b (m/z) calcd, 3039.6; observed $[M - 3H]^{3-}$ = 1012.2; found, 3039.6. ODN1_c (m/z) calcd, 3023.6; observed $[M - 3H]^{3-}$ = 1006.9; found, 3023.7. ODN2_a (m/z) calcd, 3239.6; observed $[M - 4H]^{4-}$ = 808.9; found, 3239.6. ODN2_b (m/z) calcd, 3239.6; observed $[M - 4H]^{4-}$ = 808.9; found, 3239.6. ODN2_c (m/z) calcd, 3023.6; observed $[M - 3H]^{3-}$ = 804.9; found, 3223.6.

Thermal Melting. UV melting studies were carried out on a Cary 300-Bio UV−visible spectrophotometer equipped with a 6 × 6 Multicell Block Peltier, stirrer, and temperature controller with Probe Series II. Equal amounts (0.5 A_{260}/mL each) of ODN1 or ODN2 and the complementary strands ODN1′(N) or ODN2′(N) (N = C, G, T, A) were dissolved in 0.4 mL of buffer (200 mM NaCl, 50 mM triethylamine acetate, pH 7.2, and 1 mM EDTA). The UV absorption at 260 nm was monitored as a function of temperature. Samples were heated to 85 °C for 3 min, and then, the temperature was decreased at a rate of 0.5 °C/min from 85 to 5 °C. A typical melting experiment consisted of forward/reverse scans and was repeated three times. Reverse temperature scans showed no hysteresis. The T_m values were calculated by determining the first derivative of the melting curve and were reproducible within ±1.0 °C of the reported values.

Circular Dichroism (CD) and Emission Spectra of Oligonucleotides. CD measurements were obtained on a Jasco J-815 CD spectrometer at 5 °C in 10 mM triethylamine acetate, pH 7.1, 200 mM NaCl, and 0.5 A_{260}/mL of each oligonucleotide. Samples were scanned from 400 to 200 at 0.5 nm intervals averaged over 1 s in a 1 mm light path quartz cuvette. Fluorescence emission spectra were recorded at 5 °C on a Cary Eclipse Fluorescence Spectrophotometer in 10 mM triethylamine acetate, pH 7.1, 200 mM NaCl, containing 1 μM duplex using excitation at 280 nm. All fluorescence spectra were recorded with excitation and emission slit widths kept constant at 2.5 nm.

Computational Details. In molecular dynamics (MD) simulations of the oligonucleotides, parameters for the adducts were taken from the parmbsc0[47] force field with the exception of certain dihedral parameters for the phenoxyl moiety, which were adopted from previous literature (see the Supporting Information for additional details).[48] ANTECHAMBER 1.4[49] was used to assign atom types. The R.E.D.v. III.4[50] program was used to calculate the partial charges of the modified bases using a multiconformation and multiorientation approach, as well as the rigid-body reorientation algorithm (see the Supporting Information for partial charges).[51] Two input structures corresponding to the lowest energy *anti* and lowest energy *syn* structures previously identified in the literature[41] were used in the multiconformation approach. Intermolecular charge constraints between the nucleoside sugar moiety and a dimethlyphosphate group were used, as well as intermolecular charge equivalencing procedures,[50] to obtain partial charges for the sugar moiety in the adducts analogous to the four natural nucleosides in the parm99[52] force field. Partial charges were obtained from a two stage RESP fitting and Hartree−Fock single-point calculations with the 6-31G(d) basis set using the RED code interfaced with Gaussian 03[53] and ANTECHAMBER 1.4.[49]

Simulations were carried out using the SANDER module of the AMBER 10[54] or 11[55] software packages. The parmbsc0 modification[47] to the parm99[52] force field was used since this is the most recently developed force field for nucleic acids. Initial structures were prepared using the NAB program[54] and GaussView[56] to modify the C8-PhOH-dG residue (see the Supporting Information for initial duplex structures). The LEaP module of AMBER 10 was used to prepare the systems for MD. The (natural or modified) DNA strand was neutralized with 18 sodium ions and solvated with an 8 Å TIP3P octahedron water box.[57] Coulombic interactions were approximated using the particle-mesh Ewald method,[58] bonds involving hydrogen atoms were constrained using the SHAKE option,[59] and a 2 fs time step was used throughout the simulation. A 10 Å cutoff was applied to Lennard−Jones interactions, and periodic boundary conditions were implemented. Five

Table 1. Photophysical and Redox Parameters for C-Linked Nucleoside Adducts

adduct	λ_{max} (nm), log ε[b]	λ_{em} (nm),[b] Φ_{fl}[c]	λ_{em} (nm),[d] I_{rel}[e]	$E_{p/2}$ (V/SCE)[f]
p-PhOH-dG	278, 4.26	390, 0.47	371, 0.03	0.85
o-PhOH-dG	276, 4.25	395, 0.44	375, 467, 0.25	0.98
Ph-dG	276, 4.25	393, 0.44	375, 0.07	1.06
dG[a]	253, 4.14	334, 9.7×10^{-5}		1.14

[a] Optical data for dG taken from ref 64. [b] Determined in aqueous 10 mM MOPS buffer, pH 7.0, μ = 0.1 M NaCl. [c] Determined using the comparative method with quinine bisulfate in 0.5 M H_2SO_4 (ϕ_{fl} = 0.55). [d] Emission data recorded in $CHCl_3$. [e] Relative fluorescence emission intensity in $CHCl_3$ as compared to MOPS buffered water. [f] Half-peak potentials in volts vs SCE using CV in 0.1 M TBAF in anhydrous DMF with a glassy carbon working electrode.

hundred steps of steepest descent minimization followed by 500 steps of conjugate gradient minimization were performed with the solute held fixed using a force constant of 500 kcal mol^{-1} $Å^{-2}$. Subsequently, 1000 steps of steepest descent minimization followed by 1500 steps of conjugate gradient minimization were performed on the entire system. The system was heated from 0 to 300 K using the Langevin thermostat with the solute restrained using a force constant of 10 kcal mol^{-1} $Å^{-2}$ over 20 ps under constant volume conditions. Following heating, a total of 20 ns of unrestrained MD simulations was carried out on each system under constant temperature (300 K) and pressure (1 atm) conditions. Snapshots were taken every 500 fs, and average structures were calculated from the final 2 ns of the simulation. Plots of rmsd vs time are available in the Supporting Information to show the stability of the simulations.

H-bonding interactions were calculated for MD structures obtained by averaging the coordinates of the frames from the final 2 ns of the trajectory, and replacing the backbone and surrounding bases with a hydrogen atom. ΔE_{Hbond} is calculated using counterpoise-corrected B3LYP/6-311+G(2df,p) energies. Stacking interactions were similarly calculated for MD structures obtained by averaging the coordinates of the frames that occupy the range of θ values in the most populated minimum region (shown in histograms of θ distributions, see the Discussion) of the adduct and replacing the backbone and surrounding bases with an H atom. Stacking binding strengths were calculated with M06-2X/6-31+G(d,p) since this combination has been shown to produce reliable interaction energies for noncovalent interactions with large dispersion components.[60] $\Delta E_{Int5'}$ is defined as the interaction energy between X and the 5′-flanking base (G for ODN2 or T for ODN1), while $\Delta E_{Int3'}$ is the interaction energy between X and the 3′-flanking base (A for ODN2 or C for ODN1). All (gas phase) interaction energies are calculated as the energy difference between the dimer and the individual monomers in the dimer geometry. All DFT calculations were performed with Gaussian 03[53] or Gaussian 09.[61]

RESULTS

Photophysical and Redox Properties of Nucleoside Adducts. The optical and redox properties of *p*-PhOH-dG, *o*-PhOH-dG, and Ph-dG are given in Table 1. Absorption and emission spectra were recorded in aqueous MOPS buffer, pH 7.0, and in $CHCl_3$ to model the solvatochromic properties of the adducts in the interior of the DNA helix, given that the dielectric constant (ε = 4.9) of $CHCl_3$ is similar to that in duplex DNA (ε = 3−5).[62,63] Optical data for unmodified dG in aqueous media[64] are also included for comparison. The results show blue-shifted (~20 nm) and quenched emission for the C-linked adducts in $CHCl_3$ as compared to aqueous buffer. However, the change in solvent had little influence on the absorption maxima of the nucleoside adducts, indicating a decrease in Stokes' shift in $CHCl_3$ as compared to water. This observation is consistent

Scheme 2

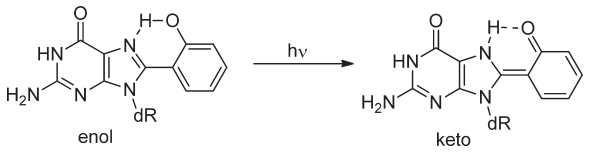

with the emitting excited state possessing a dipole moment greater than the ground state.[65] The *o*-PhOH-dG adduct also showed a peak in the emission spectrum recorded in $CHCl_3$ at 467 nm that was absent in aqueous buffer. As discussed in detail previously,[36,38] this red-shifted emission is due to the presence of the keto tautomer resulting from an excited state intramolecular proton transfer (ESIPT) process, as outlined in Scheme 2. A requirement for observation of the keto tautomer is the intramolecular H-bond between the phenolic OH and the N7 of *o*-PhOH-dG in the ground state enol structure shown in Scheme 2. That *o*-PhOH-dG shows only enol emission at 395 nm in water indicates that the intramolecular H-bond required for ESIPT is disrupted in the H-bonding solvent.

The electron donor properties of the nucleoside adducts and dG were determined using CV in anhydrous DMF, as outlined previously.[34,37] The nucleoside analogues showed irreversible 1-electron oxidation peaks with half-peak potentials ($E_{p/2}$) ranging from 0.85 V/SCE for *p*-PhOH-dG to 1.06 V for Ph-dG. Under these experimental conditions, dG gave $E_{p/2}$ = 1.14 V/SCE,[34,37] indicating that attachment of the aryl moiety enhances the electron donor characteristics of the purine nucleoside, especially when a hydroxyl group is included in the *para*-position.

DNA Melting Studies. The adducted decanucleotides ODN1_a,b,c and ODN2_a,b,c were hybridized to the complementary strands ODN1′(N) and ODN2′(N), where N is the base opposite the adduct X (Figure 1). The impact of the C-linked adducts on thermal stability of the duplex was measured using UV melting temperature analysis (T_m) with the T_m data summarized in Table 2. When N = C, the T_m data showed the C8−Ar-dG adduct to decrease helix stability (i.e., ΔT_m = −6 to −17 °C) as compared to the control unmodified duplex ($T_m \approx$ 44 °C). Introduction of a mismatch (N = G, A, and T) within the control duplexes also decreased helix stability with T_m values ranging from 25 to 31 °C (ΔT_m = −13 to −19 °C). Within the mismatched sequences, the C-linked adducts could not form stable duplexes when mismatched with A or T but could cause a stabilizing influence on the G:G mismatch. The only exception to this trend was *o*-PhOH-dG within ODN1 where a destabilization for ODN1_b:ODN1′(G) was observed (ΔT_m = −6 °C). However, for *p*-PhOH-dG and Ph-dG in both decanucleotides and

Table 2. Emission Properties and T_m Values Derived from UV Melting Experiments

ODN	T_m [a]	ΔT_m [b]	λ_{em} [c]	$\Delta\lambda_{em}$ [d]	I_{rel} [e]
ODN1_a			407	+17	0.60
ODN1_a:1′(C)	27	−17	386	−21	0.31
ODN1_a:1′(G)	31	+1	384	−23	0.22
ODN1_a:1′(A)	20	−5	400	−7	0.74
ODN1_a:1′(T)	20	−11	363	−44	0.45
ODN1_b			393	−2	0.69
ODN1_b:1′(C)	31	−13	390	−3	0.19
ODN1_b:1′(G)	24	−6	385	−8	0.16
ODN1_b:1′(A)	23	−2	389	−4	0.32
ODN1_b:1′(T)	22	−9	384, 485	−9	0.40
ODN1_c			391	−2	0.32
ODN1_c:1′(C)	31	−13	405	+14	1.66
ODN1_c:1′(G)	32	+2	390	−1	0.25
ODN1_c:1′(A)	23	−2	376	−15	2.23
ODN1_c:1′(T)	26	−5	378	−13	1.78
ODN2_a			396	+6	0.71
ODN2_a:2′(C)	28	−16	382	−14	0.42
ODN2_a:2′(G)	39	+9	395	−1	0.182
ODN2_a:2′(A)	23	−8	396	0	0.33
ODN2_a:2′(T)	21	−7	388	−8	0.29
ODN2_b			383	−12	0.88
ODN2_b:2′(C)	38	−6	380	−3	0.05
ODN2_b:2′(G)	39	+9	386	+3	0.05
ODN2_b:2′(A)	21	−4	395	+12	0.52
ODN2_b:2′(T)	23	−8	382	−1	0.75
ODN2_c			388	−5	0.15
ODN2_c:2′(C)	34	−10	386	−2	1.15
ODN2_c:2′(G)	35	+5	391	+3	0.50
ODN2_c:2′(A)	25	0	386	−2	1.37
ODN2_c:2′(T)	21	−10	385	−3	1.46

[a] In °C, determined in 50 mM triethylamine acetate, pH 7.1, 200 mM NaCl, 0.5 A_{260}/mL of each oligonucleotide. [b] Change in T_m relative to unmodified duplexes. [c] In nm, determined at 5 °C in 10 mM triethylamine acetate, pH 7.1, 200 mM NaCl. [d] Change in emission maximum for ODN1 and ODN2 vs nucleoside adducts and duplexes vs ODN1 and ODN2. [e] Relative fluorescence emission intensity for ODN1 and ODN2 vs nucleoside adducts and duplexes vs ODN1 and ODN2.

o-PhOH-dG within ODN2, T_m values ranging from 31 to 39 °C were recorded for a maximum increase in T_m of 9 °C as compared to the unmodified G:G mismatch (T_m = 30 °C). Stabilization of the G:G mismatch was greater in ODN2 (ΔT_m 5−9 °C) than ODN1 (ΔT_m 1−2 °C), suggesting that the flanking purine bases in ODN2 play a key role in the observed stabilization.

Fluorescence Emission Studies. Figure 2 shows emission spectra of ODN1_a,b,c and ODN2_a,b,c versus free nucleoside adduct in aqueous buffer. In all instances, the oligonucleotides showed quenched emission intensity as compared to the free nucleoside adducts, especially for ODN1_c and ODN2_c vs Ph-dG shown in Figure 3c (I_{rel} = 0.32 for ODN1_c, 0.15 for ODN2_c). The observed emission quenching was ascribed to π-stacking interactions of the emissive adduct with the flanking bases. The greater quenching observed for ODN2_c (flanking purine bases versus pyrimidine bases for ODN1_c) relative to the free nucleoside Ph-dG was consistent with this hypothesis.

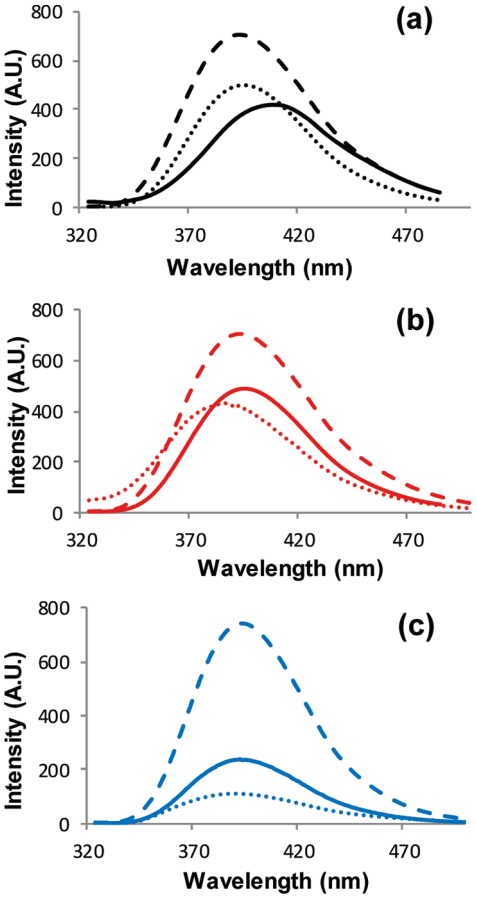

Figure 2. Fluorescence emission spectra of nucleoside adducts and oligonucleotides recorded at 5 °C in 10 mM triethylamine acetate, pH 7.1, 200 mM NaCl with excitation at 280 nm. (a) *p*-PhOH-dG (dashed black trace), ODN1_a (solid black trace), and ODN2_a (dotted black trace); (b) o-PhOH-dG (dashed red trace), ODN2_b (solid red trace), and ODN2-b (dotted red trace); and (c) Ph-dG (dashed blue trace), ODN1_c (solid blue trace), and ODN2_c (dotted blue trace).

Figure 3 shows emission spectra for the adducted decanucleotides hydridized to the complementary strands. The changes in emission maxima ($\Delta\lambda_{em}$) and relative fluorescence emission intensity (I_{rel}) for the decanucleotide strands and duplexes are included with the T_m data in Table 2. Upon hybridization, blue shifts in emission maxima were typically observed for ODN1_a-c and ODN2_a-c duplexes. This was especially the case for *p*-PhOH-dG in ODN1 (Figure 3a), where significant blue shifts were observed for duplexes involving N = C ($\Delta\lambda_{em}$ = −21 nm), G ($\Delta\lambda_{em}$ = −23 nm), and T ($\Delta\lambda_{em}$ = −44 nm), while only a blue shift of 7 nm was observed for N = A (open circles, Figure 3a). Much smaller blue shifts were observed for ODN2_a (Figure 3b), although a blue shift of 14 nm was observed for ODN2_a:ODN2′(C) (dashed trace). This general trend of greater blue shifts for duplexes involving ODN1 was also observed for the modified strands containing *o*-PhOH-dG (Figure 3c vs d) and Ph-dG (Figure 3e vs f). Given that a decrease in solvent polarity causes a blue shift in emission maxima for these adducts (Table 1), the $\Delta\lambda_{em}$ data suggested a general decrease in solvent exposure of the modified base upon duplex formation.

For the phenolic C-linked adducts (a and b), another noticeable change in fluorescence upon duplex formation was quenching. This phenomenon was dependent on the base opposite (N)

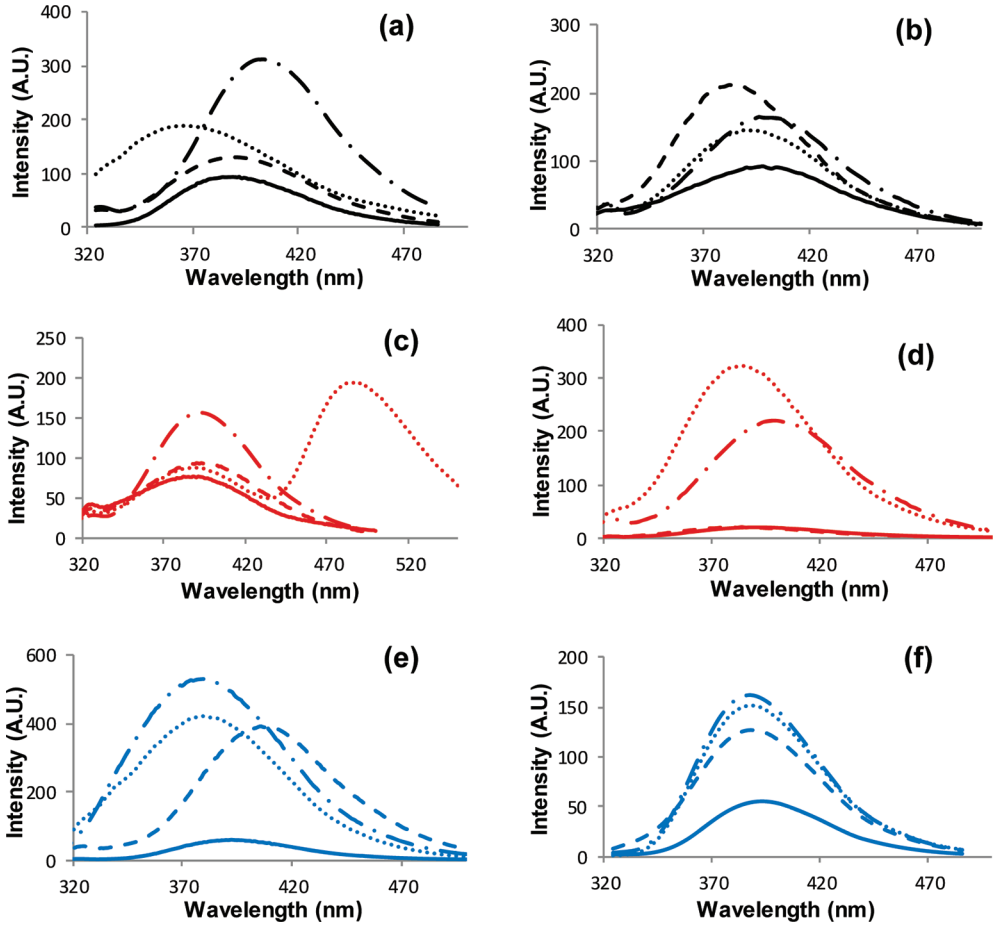

Figure 3. Fluorescence emission spectra of duplex oligonucleotides (ODN1:ODN1′ and ODN2:ODN2′) recorded at 5 °C in 10 mM triethylamine acetate, pH 7.1, 200 mM NaCl with excitation at 280 nm. (a) ODN1_a:ODN1′, (b) ODN2_a:ODN2′, (c) ODN1_b:ODN1′, (d) ODN2_b:ODN2′, (e) ODN1_c:ODN1′, and (f) ODN2_c:ODN2′, where the specific complementary strands, ODN1′ and ODN2′, are represented by N = C (dashed trace), G (solid trace), A (long dash and dot), and T (dotted trace).

the adduct, as the quenched fluorescence was typically more prominent when N = C or G, which form the more stable duplex structures. This was especially the case for ODN2_b opposite N = C or G where I_{rel} = 0.05, while opposite N = A or T, I_{rel} = 0.52, 0.72. For both C-linked phenolic adducts, greater quenching was observed within ODN2, suggesting more favorable stacking interactions with the flanking purine bases. In contrast, the fluorescence of duplexes containing Ph-dG (c) actually increased when N = C, A, and T, as exemplified for ODN1_c (N = C, I_{rel}= 1.66; N = A, I_{rel} = 2.23; and N = T, I_{rel} = 1.78).

Changes in the emission maxima also provided insight into the (*anti*/*syn*) orientation of the adduct. Particularly diagnostic in this regard was the emission spectra for *o*-PhOH-dG within ODN1 shown in Figure 3c. When mismatched with T (dotted trace), the nucleoside adduct undergoes an ESIPT process to generate the keto tautomer (Scheme 2), as indicated by the red-shifted emission peak at 485 nm. This ESIPT process for *o*-PhOH-dG was not observed in the single-strand decanucleotides (Figure 2b), nor was it observed for the other duplexes (Figure 3c,d). The observed ESIPT confirms the presence of the intramolecular H-bond between the phenolic OH and the N7 of *o*-PhOH-dG within the duplex and suggests that the Hoogsteen face of the adduct is not solvent exposed.[36,38] This observation argues strongly that *o*-PhOH-dG is in the *syn*-conformation within ODN1_b:ODN1′(T). It is also informative that the keto tautomer of *o*-PhOH-dG only occurs with the T mismatch; the only base to lack an endocyclic H-bond donor N-atom. For the other bases, Hoogsteen base pairing[42] or ESPT from the phenolic moiety to more basic nearby N-atoms could inhibit the ESIPT process.

CD. CD spectra of ODN1:ODN1′(C) and ODN2:ODN2′(C) are shown in Figure 4. The unmodified duplexes (dashed traces) show characteristics of normal B form DNA with roughly equal positive (275 nm) and negative (244 nm) bands and a crossover at ~260 nm.[66] The CD spectra of the modified duplexes for ODN2 shown in Figure 4b also show characteristics that closely resemble the normal B form helix. Greater changes in CD features were noted for the duplexes for ODN1 (Figure 4a). Here, the positive bands are slightly blue-shifted (271 nm) and broader, while the negative band is decreased in intensity and blue-shifted (224 nm). This observation suggests more distortion for duplexes involving ODN1 than ODN2. Unfortunately, the C-linked adducts absorption maxima overlap with DNA absorption, and it was not possible to resolve ellipticities due to the modified bases

Computational Studies. MD simulations on the unmodified ODN1:1′(C) and ODN2:2′(C) sequences (X = G) yield DNA duplexes with average B-DNA backbone dihedral angles

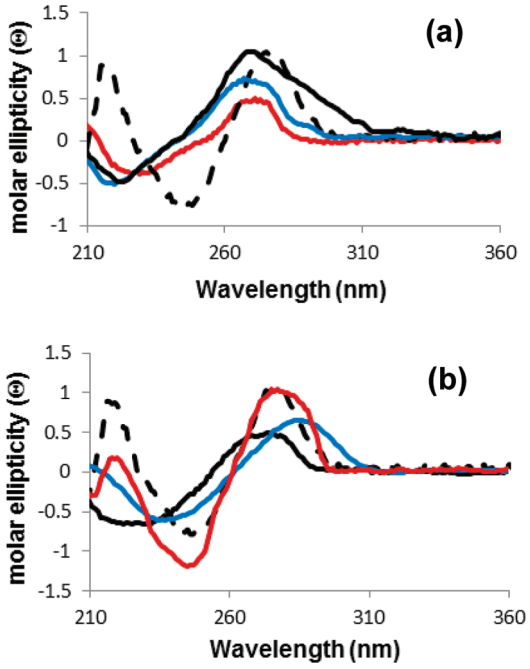

Figure 4. CD spectra of duplex oligonucleotides (N = C) recorded at 5 °C in 10 mM triethylamine acetate, pH 7.1, 200 mM NaCl. (a) Unmodified ODN1:ODN1′ (dashed), ODN1_a:ODN1′ (black), ODN1_b:ODN1′ (red), and ODN1_c:ODN1′ (blue); (b) unmodified ODN2:ODN2′ (dashed), ODN2_a:ODN2′ (black), ODN2_b:ODN2′ (red), and ODN2_c:ODN2′ (blue).

(Table S1 in the Supporting Information) and three highly occupied (~99%) Watson−Crick H-bonds between X and C. The average structure of the X:C base pair has a stability of −106.7 kJ/mol for ODN1 and −108.7 kJ/mol for ODN2 (Table 3). When X = *anti* (*syn*) G is mispaired with *syn* (*anti*) G, two strong G:G (~50 kJ/mol) Hoogsteen bonds form with 68 (93) and 96 (93)% occupancy in ODN1:1′ and 93 (68) and 93 (96)% occupancy in ODN2:2′ (Table S2 in the Supporting Information). The strands containing the mispair are likely less stable than native DNA helices due to weaker G:N H-bond strengths (by approximately 50 kJ/mol, Table 3). The strength of stacking interactions between X = G and the 5′-flanking base is −12 kJ/mol in ODN1:1′(C) and −6 kJ/mol in ODN2:2′(C), while the interactions with the 3′-flanking base are −50 kJ/mol in ODN1:1′(C) and −25 kJ/mol in ODN2:2′(C). For G:G mismatches, the stacking interactions range between −13 and −27 kJ/mol for the 5′-flanking base and −6 and −42 kJ/mol for the 3′-flanking base. The calculated interaction strengths for these unmodified bases compare very well to values reported in the literature[42,67−71] and, therefore, provide a benchmark for comparison to the binding strengths of the adducts.

When X is modified to the *o*-PhOH- or *p*-PhOH-dG adduct, no large structural changes occur to the double helix. The strands retain average values of B-DNA backbone dihedral angles with the exception of some local distortion at the site of the adduct (Table S1 in the Supporting Information). All natural and modified bases remain within the helix regardless of the (*anti* or *syn*) conformation adopted (Figure 5). Thus, although intercalation of related bulky adducts that adopt the *syn*-conformation into the helix can displace the opposing base,[30,31] the relatively small size of the C8-phenyl group is well accommodated opposite another base within the helix. However, the structure of the adduct nucleotide can significantly deviate from that predicted by smaller (nucleoside and nucleotide) computational models.[41] In particular, the dihedral angle θ describing the relative orientation of the phenoxyl group and the dG moiety can vary widely with the adduct, the sequence, and the (*anti*/*syn*) orientation. Therefore, further details of the structure of each adduct in each sequence when paired with C or mismatched with G will be discussed below. H-bond stabilities and occupancies (percentage of the total simulation time) will also be presented, where greater occupancies represent more stable H-bonds. In addition, the strength of (intrastrand) stacking interactions will be discussed to aid the determination of sequence effects on adduct structure and stability.

Table 3. DFT Interaction Energies (kJ mol^{-1}) in Average Conformations Obtained from MD Simulations

conformation	X	N	strand	$\Delta E_{\mathrm{Hbond}}$ [a]	$\Delta E_{\mathrm{Int5'}}$ [b]	$\Delta E_{\mathrm{Int3'}}$ [c]
anti	G	C	ODN1	−106.7	−12.2	−50.1
			ODN2	−108.7	−6.0	−24.8
		G	ODN1	−49.9	−22.5	−42.9
			ODN2	−50.5	−13.5	−34.4
	a	C	ODN1	−105.6	−17.3	−51.6
			ODN2	−106.4	−18.6	−37.7
		G	ODN1	−22.7	−15.5	−46.3
			ODN2	−49.0	−12.6	−33.6
	b	C	ODN1	−105.3	−10.1	−59.7
			ODN2	−107.1	−14.9	−39.1
		G	ODN1	−26.3	−19.7	−54.2
			ODN2	−55.7	−13.0	−33.7
syn	G	C	ODN1	N/A	N/A	N/A
			ODN2	N/A	N/A	N/A
		G	ODN1	−50.5	−13.8	−6.3
			ODN2	−49.9	−27.9	−13.4
	a	C	ODN1	−35.5	−16.6	−7.0
			ODN2	−3.6	−55.8	−18.2
		G	ODN1	−46.9	−16.5	−14.2
			ODN2	−48.2	−35.5	−19.9
	b	C	ODN1	6.0	−13.5	−6.6
			ODN2	−24.7	−36.5	−27.3
		G	ODN1	−45.5	−16.8	−7.9
			ODN2	−41.3	−44.0	−20.4

[a] $\Delta E_{\mathrm{Hbond}}$ is calculated as the counterpoise-corrected B3LYP/6-311+G(2df,p) H-bond strength between the dimer consisting of X and N. [b] $\Delta E_{\mathrm{Int5'}}$ is defined as the M06-2X/6-31+G(d,p) interaction energy between X and the 5′-flanking base (G for ODN2 or T for ODN1). [c] $\Delta E_{\mathrm{Int3'}}$ is defined as the M06-2X/6-31+G(d,p) interaction energy between X and the 3′-flanking base (A for ODN2 or C for ODN1).

anti-Conformation of Adducts (X = a or b) for N = C. When the phenolic adducts (a and b) adopt the *anti*-conformation in ODN1:1′(C) and ODN2:2′(C), the bulky phenoxyl group is located in the major groove (Figure 5, far left). Three strong (~−100 kJ/mol, Table 3) Watson−Crick H-bonds are intact between X:C (98−100% occupancy, Tables 4 and 5 and Figure 6a). Stacking between X and the flanking bases is generally stronger as compared to the unmodified sequences (by up to 14 kJ/mol, Table 3). However, the adduct structure is sequence dependent. For ODN2, the average θ of both adducts throughout the simulation (~220−225°, Figures 7 and 8) is similar to

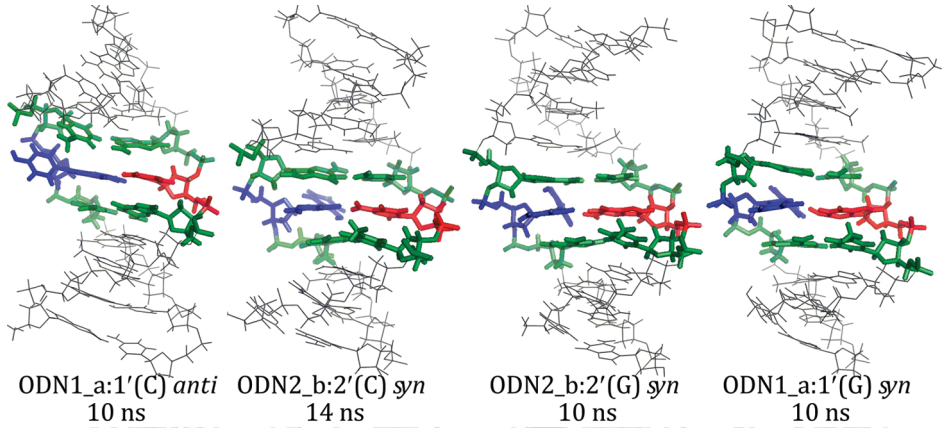

Figure 5. Examples of MD snapshots showing the view into the major groove of the B-DNA structure of the modified ODN1 and ODN2 duplexes with X = *p*-PhOH-dG (a) or *o*-PhOH-dG (b) (blue) paired opposite N = C or G (red) (purine or pyrimidine flanking bases highlighted in green).

Table 4. Hydrogen-Bond Occupancies for X = a over the Duration of MD Simulations

N	strand	adduct conformation	H-bond[a]	%
C	ODN1	*anti*	N2−H1···O2	100.0
			N1−H···N3	100.0
			N4−H1···O6	98.9
		syn	N4−H2···O6	72.4
			N4−H1···N7	43.1
	ODN2	*anti*	N2−H1···O2	99.7
			N1−H···N3	99.9
			N4−H1···O6	99.0
		syn	N4−H1···O6	39.3
			N4−H1···N7	23.2
G	ODN1	*anti*	N2−H1$_a$···N7	92.3
			N1−H$_a$···O6	56.5
			N1−H$_a$···N7	45.0
		syn	N1−H···O6$_a$	96.5
			N2−H···N7$_a$	94.9
	ODN2	*anti*	N1−H$_a$···O6	82.7
			N2−H1$_a$···N7	86.1
		syn	N1−H···O6$_a$	94.0
			N2−H1···N7$_a$	92.9

[a] Data are provided for H-bonds within 3.40 Å heavy atom separation and 120° X−H−X angle for greater than 20% of the total simulation time. To distinguish between X:G mismatches, atoms belonging to the adduct are denoted with a subscript "a".

Table 5. Hydrogen-Bond Occupancies for X = b over the Duration of MD Simulations

N	strand	adduct conformation	H-bond[a]	%
C	ODN1	*anti*	N1−H···N3	99.9
			N2−H···O2	99.6
			N4−H1···O6	98.5
			3′-N4−H···O11	65.4
		syn	O−H···N7	95.1
			N4−H1···O6	61.1
			N4−H2···O6	36.6
	ODN2	*anti*	N2−H···O2	99.8
			N1−H···N3	99.9
			O−H···N7	89.8
			N4−H···O6	98.4
		syn	O−H···N7	91.9
			N4−H1···O6	72.7
			N4−H2···O6	22.0
G	ODN1	*anti*	N2−H1$_a$···N7	75.6
			N1−H$_a$···O6	49.2
			N1−H$_a$···N7	47.7
		syn	N1−H···O6$_a$	97.2
			O−H···N7	95.9
			N2−H1···O6$_a$	76.7
			N2−H1···N7$_a$	57.2
	ODN2	*anti*	N1−H1$_a$···O6	89.2
			N2−H1$_a$···N7	73.7
			O−H···N7	45.4
			N2−H1$_a$···O6	30.7
		syn	N1−H···O6$_a$	76.9
			N2−H1···N7$_a$	68.2
			O−H···N7	20.9
			N2−H1···O6$_a$	39.3
			5′-N2−H2···O11	35.2

[a] Data are provided for H-bonds within 3.40 Å heavy atom separation and 120° X−H−X angle for greater than 20% of the total simulation time. To distinguish between X:G mismatches, atoms belonging to the adduct are denoted with a subscript "a".

the minimum identified using smaller computational models, which predict a small twist (by 20°)[41] for the *ortho* adduct due to a strongly stabilizing (O−H···N7) intramolecular H-bond, and only a slightly greater twist (by 31°)[41] for *p*-PhOH-dG. As a result in ODN2, the hydroxyl group of *o*-PhOH-dG remains H-bonded to N7 for 90% of the simulation (Table 5). In ODN1, *p*-PhOH-dG has three minimum conformations of θ (θ = ~40, ~220, and ~310°, respectively, Figure 7), which differ from *o*-PhOH-dG since the location of the hydroxyl group does not afford the same H-bonds. For ODN1, the θ angle in *o*-PhOH-dG is predominantly highly twisted ($\theta \approx 100°$ for the dominant conformation) throughout the majority of the simulation (Figure 8), which corresponds to a structure where the OH group is directed away from the dG nucleobase. Correspondingly, the O−H···N7 H-bond is disrupted (<20% occupancy). Instead, there is a very strong (−50 kJ/mol, Table 3) interaction

between the phenoxyl oxygen in the adduct and the flanking 3′-dC amino group for 65% of the simulation (Table 5). The difference in θ, and the corresponding difference in H-bonding patterns for *o*-PhOH-dG, within ODN1 versus ODN2 suggests that the adduct structure is dependent on the sequence. Regardless, the similarity in H-bonding and stacking between the *anti*-orientation of the adducts and the unmodified sequences may result in similar stability between the natural and the modified strands.

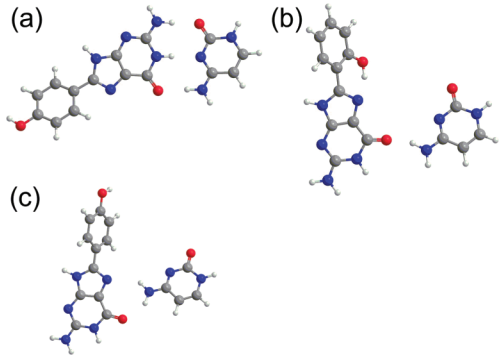

Figure 6. Average structures of H-bonded base pairs from MD simulations: (a) ODN1_a:1′(C) with the *anti*-conformation of the adduct, (b) ODN1_b:1′(C) with the *syn*-conformation of the adduct, and (c) ODN1_a:1′(C) with the *syn*-conformation of the adduct.

syn-Conformation of the Adducts (X = a or b) for N = C. When *o*-PhOH-dG adopts the *syn*-conformation within ODN1:1′(C) and ODN2:2′(C), the phenolic ring is located in the minor groove (Figure 5), and there is much greater distortion in the base pairs as compared with the corresponding *anti* pairs. This is due to the decreased stability of Hoogsteen as compared to Watson−Crick H-bonds for X:C. In fact, the (*syn*) adduct base pair is repulsive in ODN1:1′(C) (by 6 kJ/mol, Table 3) and only weakly stable in ODN2:2′(C) (by −24 kJ/mol, Table 3), due to the presence of only one (or a maximum of two) H-bonds (see, for example, Figure 6b). Specifically, N4−H of C H-bonds with O6 of the adduct for 61−73% of the simulation (Table 5). The second amino hydrogen also interacts with O6 in some configurations (22−37% occupancy, Table 5). However, a Hoogsteen H-bond involving N7 cannot form since a stable intramolecular

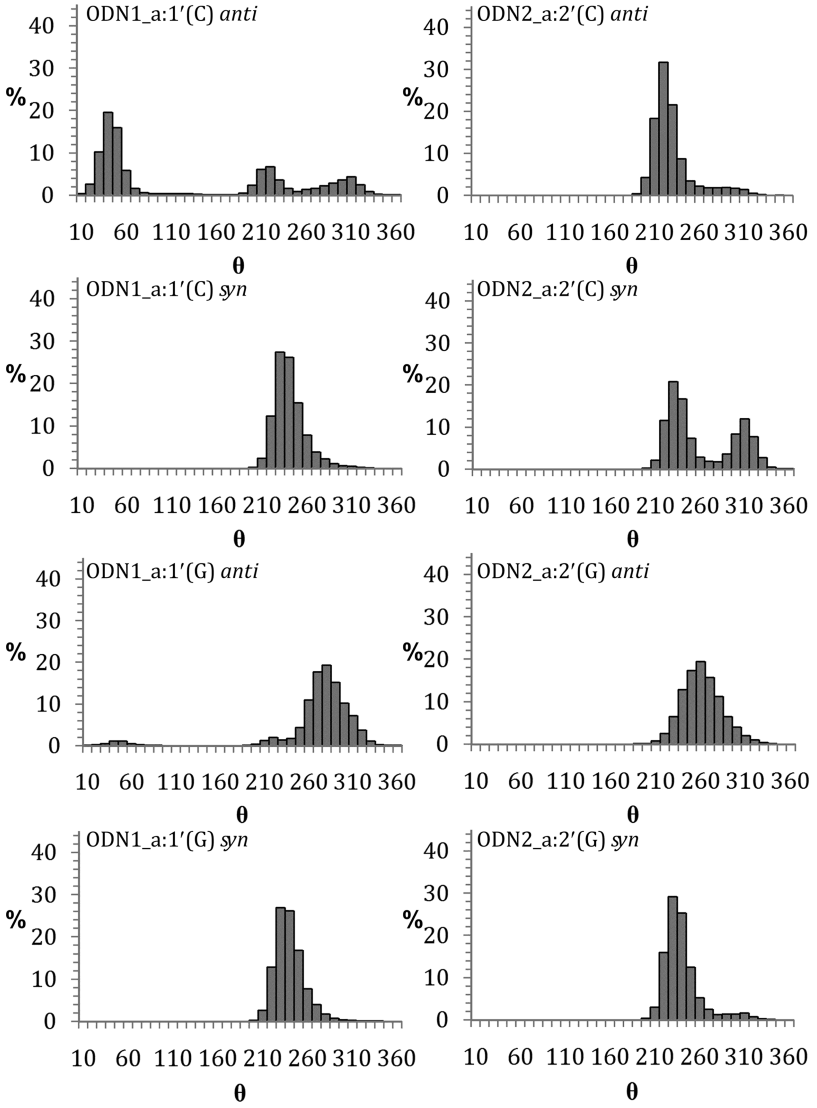

Figure 7. Percent distribution of θ (degrees) throughout the 20 ns trajectories for the *p*-PhOH-dG (a) adduct.

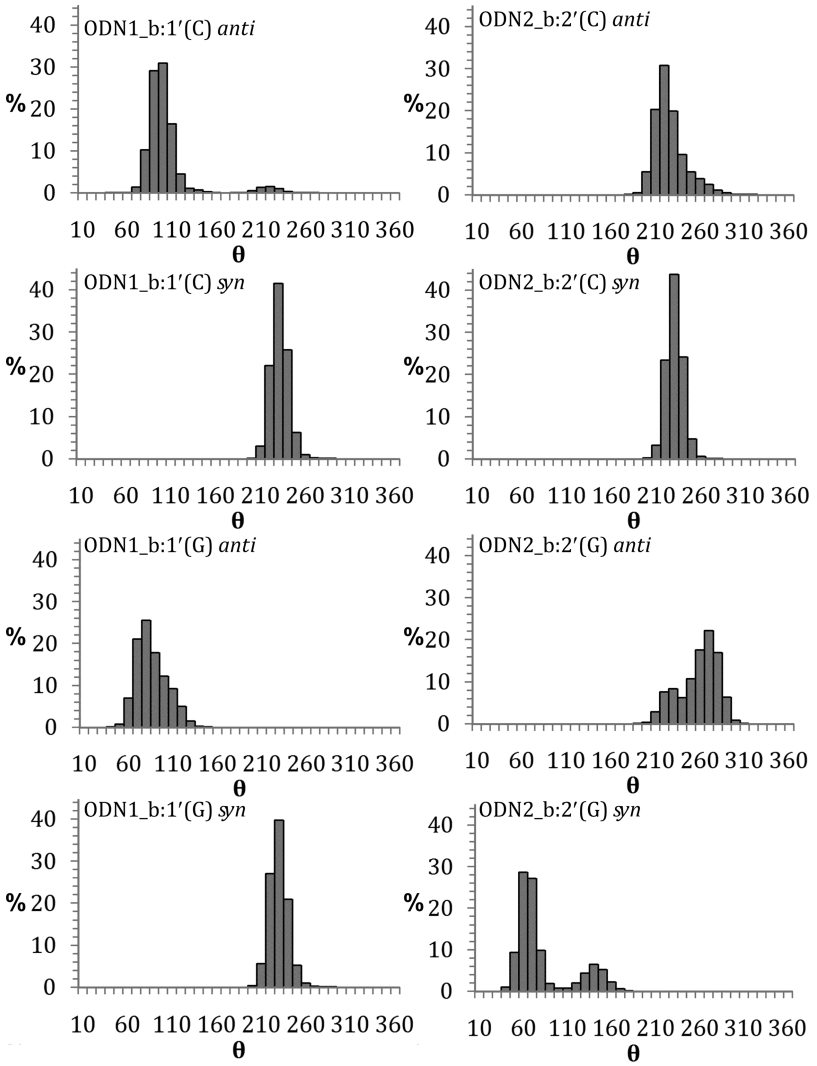

Figure 8. Percent distribution of θ (degrees) throughout the 20 ns trajectories for the *o*-PhOH-dG (b) adduct.

O−H···N7 H-bond is intact for 92−95% of the simulation. Because of the poor H-bonding between the bases, the strands are expected to be destabilized when the *syn*-conformation of the adduct is paired with C as compared with strands containing natural dG or the *anti*-adduct paired with C.

When *p*-PhOH-dG adopts the *syn*-conformation opposite C, there are some differences in Hoogsteen bonding as compared to *o*-PhOH-dG. Specifically, the Hoogsteen bond between the N4−H of C and O6 in the adduct is present for less time for *p*-PhOH-dG (8% for ODN1 and 39% for ODN2, Table 4) as compared to *o*-PhOH-dG (61−73%, Table 5). Instead, the dominant binding conformation of *p*-PhOH-dG in ODN1 involves one or two H-bonds between the N4 amino group of C and O6 (72%) and, interestingly, sometimes an interaction between N4−H of C and N7 (43%) (Figure 6c). This increased Hoogsteen bonding to N7 in ODN1 is likely due to a lack of competing O−H···N7 H-bond. This results in a base pair stability of −35 kJ/mol in ODN1 (Table 3). There is less Hoogsteen bonding to N7 in ODN2 (23%, Table 4), which leads to weaker H-bonding (−3.6 kJ/mol, Table 3), although the reason for this is currently unclear.

anti-Conformation of Adducts (X = a or b) for N = G. When the adducts adopt the *anti*-conformation opposite *syn*-G, two H-bond contacts occur between the Watson−Crick face of the adduct and the Hoogsteen face of G. Specifically, the N2 amino group of the adduct bonds to N7 of G (74−92%, Tables 4 and 5) and N1−H of the adduct bonds to O6 of G (49−89%). However, as compared to the unmodified G:G mismatch, the Hoogsteen base pair strength is considerably weaker for the modified ODN1:1′(G) (−23 to −26 kJ/mol as compared to −50 kJ/mol, Table 3) but comparable for ODN2:2′(G) (−49 to −56 kJ/mol, Table 3). As found when the *anti*-adducts are paired with C, the θ twist is dependent on both the sequence and the adduct. For ODN1_a:1′(G), three minimum conformations of θ occur at θ = ∼280, 220, and 50°, and there is a single conformation (θ = 256.5°, Figure 7) for ODN2_a:2′(G). These values correspond to a highly twisted structure regardless of sequence for *p*-PhOH-dG. For *o*-PhOH-dG, an average θ value of ∼80° occurs for ODN1:1′(G) (Figure 8), which corresponds to a highly twisted structure (similar to *p*-PhOH-dG) with no O−H···N7 H-bond (within the cutoff criteria, Table 5). For ODN2:2′(G), two minima θ conformations occur (Figure 8). In the first (θ ∼ 230°), the O−H···N7 H-bond is intact (45%, Table 5), while the phenoxyl group rotates (θ ∼ 270°) in the second conformation, which breaks or significantly weakens the

dx.doi.org/10.1021/tx200247f |*Chem. Res. Toxicol.* 2011, 24, 1694–1709

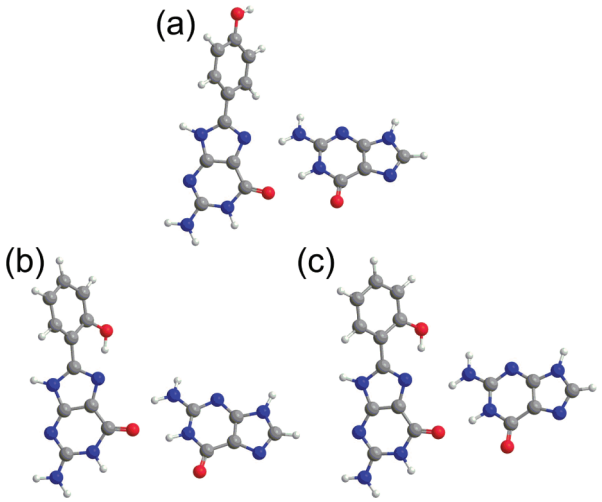

Figure 9. H-bonding in ODN1:1′(G) from MD simulation. (a) The *syn*-conformation of *p*-PhOH-dG paired with G. (b) A representative structure of the H-bonding pattern for the *syn*-conformation of *o*-PhOH-dG paired with G. (c) The average H-bonding pattern of the *syn*-conformation of *o*-PhOH-dG paired with G that overestimates the strand stability.

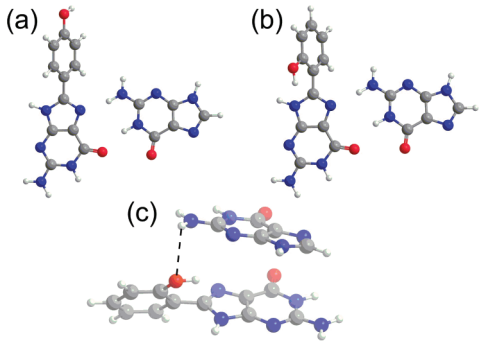

Figure 10. H-bonding in ODN2:2′(G) from MD simulation. (a) The *syn*-conformation of *p*-PhOH-dG paired with G. (b) The *syn*-conformation of *o*-PhOH-dG paired with G. (c) The H-bonding interaction between *o*-PhOH-dG and the 5′-flanking G base.

O−H···N7 H-bond. These changes in θ lead to adduct stacking interactions ranging between −13 and −20 kJ/mol with the 5′-flanking base and −34 and −54 kJ/mol with the 3′-flanking base (Table 3). In general, the magnitudes of the stacking interactions for the adducts and the unmodified G:G mismatch are similar, although *o*-PhOH-dG shows a greater interaction with the 3′-flanking base within ODN1 as compared to the G:G mismatch (−54 vs −43 kJ/mol, Table 3). These calculated structures for *anti*-adduct:*syn*-G within ODN1 predict a more stable structure for *o*-PhOH-dG versus *p*-PhOH-dG and that both should be less stable than the unmodified G:G mismatch due primarily to the significant drop in H-bonding stability.

syn-Conformation of the Adducts (X = a or b) for N = G. When the adducts adopt the *syn*-conformation opposite *anti*-G, there is not a dramatic drop in Hoogsteen H-bonding stability as compared with the natural helices as discussed above for ODN1 strands with the *anti*-adduct opposite *syn* G. For *p*-PhOH-dG, two strong (−46 to −48 kJ/mol, Table 3) Hoogsteen bonds (92−96%, Table 4) form between the adduct and G regardless of the sequence (Figures 9a and 10a), which are only slightly less stable than the unmodified G:G mismatch (−50 kJ/mol, Table 3). The duplexes containing *o*-PhOH-dG show a slightly greater decrease in H-bonding stability (−41, −45 as compared to −50 kJ/mol, Table 3). For ODN1, N1−H of the Watson−Crick face of G H-bonds to O6 of the *ortho* adduct (97%, Table 5), and a second N2−H···O6 Hoogsteen bond is present (77%), while a third Hoogsteen bond (N2−H···N7) is present for less (57%) time (Figure 9b,c). The lower percentage of Hoogsteen bonding to N7 may be related to the competing (O−H···N7) hydrogen bond (96%, Table 5). For ODN2, the two Hoogsteen bonds to O6 of *o*-PhOH-dG are less occupied (39−77%, Table 5), while the N2−H···N7 Hoogsteen bond is more occupied (68%) than ODN1 (Figure 10b). This can be correlated to a much higher degree of θ twist in ODN2 than ODN1 (predominantly 80° as compared to 225°, Figure 8). The larger twist leads to a structure with the O−H···N7 interaction disrupted and the phenoxyl group forming a N2−H···O interaction (35%, Table 5) with the 5′-flanking G base (Figure 10c). This reduces the occupation of the O−H···N7 contact (to 21%) and frees N7 to form Hoogsteen bonds.

DISCUSSION

Structural Impact of C-Linked Phenolic Adducts on Duplex DNA. The data summarized in Table 2 show the C[8]-Ar-dG adduct to destabilize the duplex when base paired with its normal partner C. This observation is in agreement with previous studies showing bulky C-linked and N-linked C[8]-Ar-G lesions to decrease duplex stability. The Wagenknecht laboratory carried out T_m studies on the C8-(pyren-1-yl)-dG modification and recorded a ΔT_m value of ∼−10 °C for the adduct when placed in the middle of the 16-mer duplex 5′-GCATCTGXATCACTGA, where X = Py-8-dG.[72] The N-linked C8-dG adducts of 2-aminofluorene (AF) and AAF also destabilize the duplex considerably when base paired with C. For the N-linked AF adduct, Elmquist and co-workers incorporated the lesion into three 12-mer oligonucleotides and showed the adduct to lower the T_m by 8−13 °C relative to the unmodified duplex.[73] For the N-linked AAF adduct, Koehl and co-workers[74] incorporated the adduct into the three G sites of the *Nar*I oligonucleotide 5′-AC-CGGCGCCACA (underlined Gs were replaced with the N-linked AAF adduct). The AAF-modified oligonucleotides showed a large destabilization with ΔT_m values of −10−13 °C.[74]

Factors thought to cause the destabilizing influence of the C-linked and N-linked C[8]-Ar-dG lesions when base paired with C depend on the conformation of the adduct. If the adduct is present in the *anti*-conformation, it can form a Watson−Crick base pair with C. This base pairing places the bulky C8-Aryl group outside the helix in the major groove, and it is not involved in base-stacking interactions. Solvent exposure of the lipophilic aryl group is thought to account for the lesion-induced duplex destabilization in the *anti*-conformation.[73,74] If the C[8]-Ar-dG adduct is present in the *syn*-conformation, then the loss of Watson−Crick base pairing with C coupled with helix distortions decreases the stability of the modified duplex.[29−31]

For the phenolic C-linked adducts, our experimental and MD simulations suggest that they adopt the *syn*-conformation with the phenolic ring located in the minor groove, similar to the W structure observed for N-linked adducts.[30] Such a minor groove conformation would account for the significant drop in duplex

stability (6−17 °C, Table 2) when these C8-Ar-dG lesions base pair with C since the *syn* base is not Watson−Crick paired. For *o*-PhOH-dG, enhanced stacking interactions (Table 3) in ODN2_b:2′(C) (*syn*-adduct) as compared to the unmodified sequence (*anti*-G) may explain why ODN2_b:2′(C) is less destabilized than ODN1_b:1′(C), which has weaker stacking relative to the unmodified sequence. Furthermore, the X:C H-bonding is more favorable in ODN2 than in ODN1 (Table 3). Comparison of the MD simulations for ODN1_a and ODN2_a to the T_m results leads to similar conclusions noted for strands containing *o*-PhOH-dG. Specifically, the decrease in stability (by 17 and 16 °C, Table 2) observed for strands containing the *p*-PhOH-dG:C pair implies that the *syn*-orientation of the adduct is present in both duplexes. Unlike *o*-PhOH-dG, there is no improved stability for ODN2_a as compared to ODN1_a, which is likely due to a cancellation in improved stacking by weakening of the H-bonds (Table 3). The fact that the adduct prefers to be in the *syn*-conformation, despite loss in stability due to weaker H-bonding, implies that other (sterics, major groove contacts, etc.) factors push the adduct to adopt a *syn*-orientation regardless of the base in the opposite strand.

The impact of duplex formation on the fluorescent properties of the C-linked phenolic adducts (Figure 3 and Table 2) also supports a *syn*-preference. Upon hybridization, blue shifts in emission maxima were typically observed. This correlates with changes in emission maxima of the nucleoside adducts in water versus $CHCl_3$ (Table 1), suggesting a decrease in solvent exposure of the modified base upon duplex formation. The emission spectrum of ODN1_b:1′(T) also gave rise to keto emission, confirming the presence of the intramolecular O−H···N7 H-bond and suggesting that the Hoogsteen face of the adduct is not solvent exposed.[36,38]

The *syn*-adduct preference is also supported by the ability of the adduct to stabilize the G:G mismatch. Experimental insight into the stabilizing influence of the phenolic C-linked adducts on the G:G mismatch comes from work on G-quadruplex formation. A G-quadruplex can form with alternating *syn*- and *anti*-conformation of G bases.[75] Because the addition of bulky groups to C8-dG can shift the conformational equilibrium of the glycosidic bond from *anti* to *syn*, replacement of *syn* Gs within the G-quadruplex with C8-Ar-dG adducts that favor the *syn*-conformation can be used to stabilize the quadruplex.[76,77] Incorporation of 8-Br-dG into G-quadruplexes has been shown to stabilize the quadruplex by 4−13 °C.[76] More recently, Dumas and Luedtke[77] incorporated a C8-pyridyl-dG into G-quadruplex-folding oligonucleotides and demonstrated the utility of the nucleobase to stabilize the G-quadruplex due to the *syn*-conformational preference of the C8-pyridyl adduct. The impact of C8-pyridyl-dG on G-quadruplex formation (ΔT_m = +10 °C) was found to correlate with the ΔT_m values recorded for the C-linked phenolic adducts ODN2_b:2′(G) and ODN2_c:2′(G) (ΔT_m = +9 °C) given in Table 2.

It is interesting that the T_m data show that the G mismatch with *p*-PhOH-dG is more stable than that with *o*-PhOH-dG in ODN1:1′(G). The *syn p*-PhOH-dG:G base pair in ODN1:1′(G) involves two H-bonds between N1−H of G and O6 of the adduct (96%) and N2−H of G and N7 of the adduct (95%) (Figure 9a). This is similar to the natural unmodified sequence, where N7 is free to form Hoogsteen bonds. Thus, ODN1_a:1′(G) and the unmodified G:G mismatch have similar stabilities (ΔT_m = +1 °C, Table 2). However, the stability of ODN1_b:1′(G) is quite different. Specifically, because O−H···N7 is highly populated (96%), N7 is not as available to form Hoogsteen bonds. In fact, only one Hoogsteen bond (N1−H···O6) is occupied for the majority of the simulation (97%), while G-N2−H bonds to N7 of the adduct 57% of the time. For some of the simulation (77%), G-N2−H also H-bonds to O6 (Figure 9b). In addition, both of the latter interactions involve >3 Å average distance for *o*-PhOH-dG but less than 3 Å for *p*-PhOH-dG or natural G. Therefore, *p*-PhOH-dG is expected to form a much more stable base pair with G than *o*-PhOH-dG in ODN1:1′(G). This is not reflected in the calculated values for H-bond strengths (Table 3) since the average structure of ODN1_b:1′(G) contains three weak H-bonds even though the dominant conformation contains only one strong interaction (Figure 9c). The decrease in Hoogsteen binding to N7 also explains why ODN1_b:1′(G) is destabilized with respect to the natural G:G mismatch (by −6 °C, Table 2).

The stability of *p*-PhOH-dG:G and *o*-PhOH-dG:G base pairs is also sequence dependent. ODN2_a:2′(G) and ODN2_b:2′-(G) are stabilized to the same degree (+9 °C) with respect to the unmodified G:G mismatched sequences. Close examination of the base pairs throughout the simulation reveals that two Hoogsteen N1−H···O6 (94%) and N2−H···N7 (93%) *p*-PhOH-dG H-bonds are not affected by the sequence (Figure 10a). However, *o*-PhOH-dG forms two strong Hoogsteen bonds in ODN2:2′ (Figure 10b) but only one in ODN1:1′ (Figure 9b). Specifically, N1−H···O6 (77%) and N2−H···N7 (68%) are both present in ODN2, which is more similar to the bonding in the *p*-PhOH-dG and unmodified duplexes (68−96%). In ODN1_b:1′(G), N7 is blocked from forming strong bonds due to the stability of O−H···N7 (96%). However, in ODN2_b:2′(G), the O−H···N7 bond is present only 21% of the simulation, which allows for Hoogsteen bonding to occur during the remainder of the simulation. This effect is sequence specific since the H-bond is broken due to formation of a weak N2−H···O contact (35%) between the 5′-flanking G and the phenoxyl oxygen (Figure 10c), which distorts θ (76.7°). This provides a possible explanation for the observed relative stabilities of ODN2_a:2′(G) and ODN2_b:2′(G) (Table 2).

The interaction of the phenolic OH in *o*-PhOH-dG with the 5′-flanking G in ODN2 also provides a rationale for the inability to detect keto emission for duplexes involving ODN2_b (Figure 3d), even though *o*-PhOH-dG is predicted to be in the *syn*-conformation and is not solvent exposed. A similar argument has been proposed by the Romesberg laboratory for the inability to detect keto emission in a 2-(2′-hydroxyphenyl)benzoxazole (HBO) artificial nucleoside.[78] When incorporated into the major groove opposite an abasic site, the HBO nucleobase undergoes ESIPT to generate keto emission. However, upon incorporation of the HBO base with the enol moiety positioned in the minor groove, formation of a stable H-bond between the phenolic OH and the 3′-flanking sugar O4′ atom inhibits the ESIPT process to generate only enol emission.[78]

The increase in stability of the modified G:G mismatch within ODN2 may be due to the enhanced stacking of the *syn*-adduct with purine bases as compared with the pyrimidine bases (Table 3). Stronger stacking arises since the phenoxyl group is involved in stacking and T-shaped interactions with the flanking bases in ODN2 (Figure 11a,b) but to a lesser extent in ODN1. Indeed, the pyrimidine bases are too small to overlap with the entire adduct and, therefore, only interact with dG in a manner similar to the natural strand (Figure 11c,d). The stacking strengths calculated for the *syn*-orientations of the adducts (Table 3) support enhanced stability of ODN2:2′ upon incorporation of both

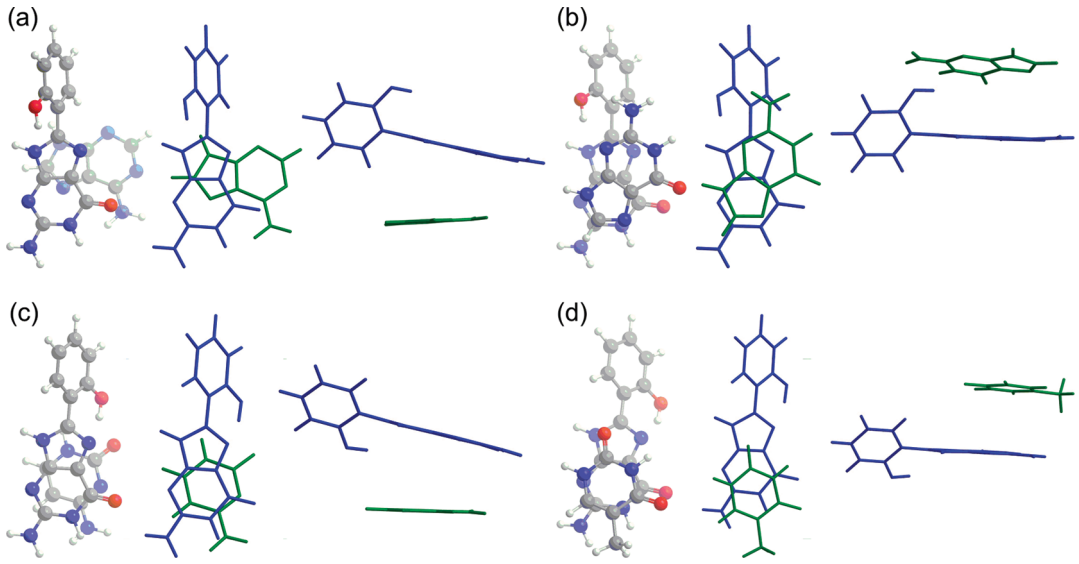

Figure 11. Face (left, center) and edge (right) views of the intrastrand stacking interactions between *o*-PhOH-dG and the 3′- (a, c) or 5′- (b, d) flanking base in the ODN2:2′ (a, b) and ODN1:1′ (c, d) sequences.

adducts. Greater fluorescence quenching for the C-linked phenolic adducts was also observed within ODN2, suggesting more favorable stacking interactions with the flanking purine bases.

Biological Implications of C-Linked Phenolic Adducts. For the N-linked C8-dG adducts, biological outcome in terms of mutagenicity appears to be strongly correlated to the conformational preference of the adduct.[29] The duplex DNA structures containing N-linked adducts base paired with C can be minimally perturbed with the adduct present in the *anti*-conformation with the N-linked aryl ring located in the major groove. Alternatively, the *syn*-adduct structures have the N-linked aryl ring intercalated into the helix with local unwinding and with displacement of the modified G. The equilibrium between the two conformers is highly sequence-dependent,[30,31,73,74] which generates mutagenic hotspots.[29] Because DNA repair enzymes seek out distorting lesions as substrates, the minimally perturbed *anti*-conformer structures are less repair-prone.[29] However, the *syn*-conformer adduct structures are relevant to mutagenic replication and provide a rationale for the propensity of N-linked C8-dG adducts to induce frameshift mutations by stabilizing bulges through formation of the base-displaced intercalated structures.[29] The *syn*-adduct structures also provide a rationale for misincorporation of A opposite the modified G base.[29]

For the C-linked phenolic adducts in the *syn*-conformation, our MD simulations suggest that the C8-phenyl group is located in the minor groove within the helix and the C base is not flipped out, as noted for the corresponding N-linked adducts.[29] This observation is important in terms of biological activity, as it suggests that the C-linked phenolic adducts will be less able to stabilize bulges that are important for inducing frameshift mutations. Our MD simulations also suggest that the C-linked phenolic adducts minimally perturb the B-form duplex DNA structure. These finding imply that the C-linked phenolic adducts may be less repair-prone than the corresponding N-linked adducts, which cause major distortion to the duplex in the base-displaced intercalated structure.[29]

While the biological activity of C-linked phenolic adducts has yet to be addressed, primer-extension assays have been performed for 8-Ph-dG within a single 24-mer oligonucleotide with the lesion flanked by pyrimidine bases (C).[79] UV thermal melting experiments were also performed for 8-Ph-dG within the 12-mer sequence 5′-d(GCGCCXGCGGTG), where X = 8-Ph-dG. Unfortunately, the thermal melting data contained the lesion flanked by C and G, which does not correlate with the sequence used for the primer-extension assays.[79] Within the 12-mer, the T_m of the duplex was 5.6 °C lower than the normal G:C base pair, while the T_m of 8-Ph-dG:G was 2.1 °C higher than that of the mismatched G:G base pair, again highlighting the ability of 8-Ph-dG to stabilize a G:G mismatch. Klenow fragment from *E. coli* incorporated predominately the correct base dCMP opposite 8-Ph-dG, while primer extension by mammalian pol α was strongly blocked opposite the lesion. Small amounts of dGMP and dAMP were incorporated opposite the lesion; two-base deletions were also observed, suggesting that 8-Ph-dG is weakly mutagenic capable of generating G→C and G→T transversions and deletions in cells.

The results of our studies suggest that C-linked phenolic adducts could show hotspots for mutagenicity. The lesions are better able to stabilize G:G mismatches when flanked by purine bases. Thus, purine-rich sites would be expected to show a greater propensity for misincorporation of G, as the mismatched G can be stably accommodated opposite the *syn*-adduct within the duplex.

In summary, we have demonstrated the structural impact of C-linked phenolic adduct within two decanucleotide substrates. The C8-dG adducts decrease duplex stability (6−17 °C) when base paired with C but show a sequence-dependent increase in duplex stability when mismatched with G (5−9 °C). Stabilization of the G:G mismatch by the C-linked phenolic adducts was greater in the decanucleotide containing flanking purine bases, suggesting more favorable stacking interactions with the flanking purine bases, as opposed to the smaller pyrimidines. MD simulations and changes in fluorescent emission of the adducts upon hybridization to the complementary strands implied a *syn*-conformation preference for the adducts within both duplexes regardless of the opposite base N. The *syn*-preference of the adducts coupled with their ability to stabilize G:G mismatches in a sequence specific fashion suggests the possibility for C-linked

phenolic adducts to display mutagenic hotspots, as noted for the corresponding N-linked C8-dG adducts derived from arylamine carcinogens.

■ ASSOCIATED CONTENT

Supporting Information. Table S1 containing average backbone values according final snapshots from MD simulations, Table S2 containing H-bond occupancies for the natural helices, Tables S3 and S4 containing average distances and angles for H-bond occupancies of the adducts, mol2 files for modified bases with partial charges and atom types, additional parameters for modified bases, HPLC traces and MS spectra for ODN1_a,b,c and ODN2_a,b,c, figures of MD snapshots, and figures of rmsd plots for MD simulations; files of duplex starting structures available in separate file in pdb format; and Cartesian coordinates for average MD structures used in DFT calculations available upon request. This material is available free of charge via the Internet at http://pubs.acs.org.

■ AUTHOR INFORMATION

Corresponding Author

*E-mail: stacey.wetmore@uleth.ca (S.D.W.). E-mail: rmanderv@uoguelph.ca (R.A.M.).

Author Contributions

§These authors contributed equally to this work.

Funding Sources

Support for this research was provided by the Natural Sciences and Engineering Research Council (NSERC) of Canada, the Canada Research Chair program, the Canada Foundation for Innovation, and the Ontario Innovation Trust Fund. A.L.M. also thanks Alberta Ingenuity, now part of Alberta Innovates—Technology Futures.

■ ACKNOWLEDGMENT

R.A.M. thanks Katherine M. Schlitt and Christopher K. McLaughlin for carrying our preliminary experiments. This research has been facilitated by use of computing resources provided by WestGrid and Compute/Calcul Canada.

■ ABBREVIATIONS

dG, 2′-deoxyguanosine; Ar, aryl; CD, circular dichroism; MD, molecular dynamics; *p*-PhOH-dG, 8-(4″-hydroxyphenyl)-dG; *o*-PhOH-dG, 8-(2″-hydroxyphenyl)-dG; Ph-dG, 8-phenyl-dG; AAF-G, 8-acetylaminofluorene-G; ODN, oligonucleotide; TPPTS, 3,3′,3″-phosphinidynetris(benzenesulfonic acid) trisodium salt; DMF, *N*,*N*-dimethylformamide; CV, cyclic voltammetry; TBAF, tetrabutylammonium hexafluorophosphate.

■ REFERENCES

(1) Burton, G. W., and Ingold, K. U. (1986) Vitamin E: Application of the principles of physical organic chemistry to the exploration of its structure and function. *Acc. Chem. Res. 19*, 194–201.

(2) Yao, L. H., Jiang, Y. M., Shi, J., Tomas-Barberan, F. A., Datta, N., Singanusong, R., and Chen., S. S. (2004) Flavonoids in food and their health benefits. *Plants Foods Hum. Nutr. 59*, 113–122.

(3) Manderville, R. A., and Pfohl-Leszkowicz, A. (2006) Genotoxicity of chlorophenols and ochratoxin A. In *Advances in Molecular Toxicology* (Fishbein, J. C., Ed.) Vol. 1, pp 85−138, Elsevier, Amsterdam.

(4) Shadnia, H., and Wright, J. S. (2008) Understanding the toxicity of phenols: using quantitative structure-activity relationships and enthalpy changes to discriminate between possible mechanisms. *Chem. Res. Toxicol. 21*, 1197–1204.

(5) Li, C., and Hoffman, M. Z. (1999) One-electron redox potentials of phenols in aqueous solution. *J. Phys. Chem. B 103*, 6653–6656.

(6) Murray, A. R., Kisin, E., Castranova, V., Kommineni, C., Gunther, M. R., and Shvedova, A. A. (2007) Phenol-induced in vivo oxidative stress in skin: Evidence for enhanced free radical generation, thiol oxidation and antioxidant depletion. *Chem. Res. Toxicol. 20*, 1769–1777.

(7) Dai, J., Wright, M. W., and Manderville, R. A. (2003) An oxygen-bonded C8-deoxyguanosine nucleoside adduct of pentachlorophenol by peroxidase activation: Evidence for ambident C8 reactivity by phenoxyl radicals. *Chem. Res. Toxicol. 16*, 817–821.

(8) Dai, J., Sloat, A. L., Wright, M. W., and Manderville, R. A. (2005) Role of phenoxyl radicals in DNA adduction by chlorophenol xenobiotics following peroxidase activation. *Chem. Res. Toxicol. 18*, 771–779.

(9) Faucet, V., Pfohl-Leszkowicz, A., Dai, J., Castegnaro, M., and Manderville, R. A. (2004) Evidence for covalent DNA adduction by ochratoxin A following chronic exposure to rat and subacute exposure to pig. *Chem. Res. Toxicol. 17*, 1289–1296.

(10) Mantle, P. G., Faucet-Marquis, V., Manderville, R. A., Squillaci, B., and Pfohl-Leszkowicz, A. (2010) Structures of covalents adducts between DNA and ochratoxin A: A new factor in debate about genotoxicity and human risk assessment. *Chem. Res. Toxicol. 23*, 89–98.

(11) Manderville, R. A. (2009) Structural and biological impact of radical addition reactions with DNA nucleobases. In *Advances in Physical Organic Chemistry* (Richard, J. P., Ed.) pp 177−218, Elsevier, Amsterdam.

(12) Manderville, R. A. (2009) DNA damage by phenoxyl radicals. In *Radical and Radical Ion Reactivity in Nucleic Acid Chemistry* (Greenberg, M., Ed.) pp 421−443, John Wiley & Sons, Hoboken.

(13) Manderville, R. A. (2005) Ambident reactivity of phenoxyl radicals in DNA adduction. *Can. J. Chem. 83*, 1261–1267.

(14) Kikugawa, K., Kato, T., and Kojima, K. (1992) Substitution of p- and o-hydroxyphenyl radicals at the 8 position of purine nucleosides by reaction with mutagenic p- and o-diazoquinones. *Mutat. Res. 268*, 65–75.

(15) Lawson, T., Gannett, P. M., Yau, W.-M., Dalal, N. S., and Toth, B. (1995) Different patterns of mutagenicity of arenediazonium ions in V79 cells and salmonella typhimurium TA102: Evidence for different mechanisms of action. *J. Agric. Food Chem. 43*, 2627–2635.

(16) Hiramoto, K., Kaku, M., Sueyoshi, A., Fujise, M., and Kikugawa, K. (1995) DNA base and deoxyribose modification by the carbon-centered radical generated from 4-(hydroxymethyl) benzenediazonium salt, a carcinogen in mushroom. *Chem. Res. Toxicol. 8*, 356–362.

(17) Gannett, P. M., Powell, J. H., Rao, R., Shi, X., Lawson, T., Kolar, C., and Toth, B. (1999) C8-Arylguanine and C8-aryladenine formation in calf thymus DNA from arenediazonium ions. *Chem. Res. Toxicol. 12*, 297–304.

(18) Rogan, E. G., Cavalieri, E. L., Tibbels, S. R., Cremonesi, P., Warner, C. D., Nagel, D. L., Tomer, K. B., Cerney, R. L., and Gross, M. L. (1988) Synthesis and identification of benzo[a]pyrene-guanine nucleoside adducts formed by electrochemical oxidation and by horseradish peroxidase catalyzed reaction of benzo[a]pyrene with DNA. *J. Am. Chem. Soc. 110*, 4023–4029.

(19) Akanni, A., and Abul-Hajj, Y. J. (1999) Estrogen-nucleic acid adducts: Dissection of the reaction of 3,4-estrone quinone and its radical anion and radical cation with deoxynucleosides and DNA. *Chem. Res. Toxicol. 12*, 1247–1253.

(20) Enya, T., Kawanishi, M., Suzuki, H., Matsui, S., and Hisamatsu, Y. (1998) An unusual DNA adduct derived from the powerfully mutagenic environmental contaminant 3-nitrobenzanthrone. *Chem. Res. Toxicol. 11*, 1460–1467.

(21) Hoffmann, G. R., and Fuchs, R. P. P. (1997) Mechanisms of frameshift mutations: Insight from aromatic amines. *Chem. Res. Toxicol. 10*, 347–359.

(22) Leong-Morgenthaler, P. M., Op Het Velt, C., Jaccaud, E., and Turesky, R. J. (1998) Mutagenicity of 2-amino-3-methylimidazo[4,5-*f*]-quinolone in human lymphoblastoid cells. *Carcinogenesis 19*, 1749–1754.

(23) Tan, X., Suzuki, N., Grollman, A. P., and Shibutani, S. (2002) Mutagenic events in *Escherichia coli* and mammalian cells generated in response to acetylaminofluorene-derived DNA adducts positioned in the *Nar I* restriction enzyme site. *Biochemistry 41*, 14255–14262.

(24) Wang, Z., and Rizzo, C. J. (2001) Synthesis of the C8-deoxyguanosine adduct of the food mutagen IQ. *Org. Lett. 3*, 565–568.

(25) Lakshman, M. K. (2005) Synthesis of biologically important nucleoside analogs by palladium-catalyzed C-N bond-formation. *Curr. Org. Synth. 2*, 83–112.

(26) Elmquist, C. E., Stover, J. S., Wang, Z., and Rizzo, C. J. (2004) Site-specific synthesis and properties of oligonucleotides containing C8-deoxyguanosine adducts of the dietary mutagen IQ. *J. Am. Chem. Soc. 126*, 11189–11201.

(27) Böge, N., Gräsl, S., and Meier, C. (2006) Synthesis and properties of oligonucleotides containing C8-deoxyguanosine arylamine adducts of borderline carcinogens. *J. Org. Chem. 71*, 9728–9738.

(28) Bonala, R., Torres, M. C., Iden, C. R., and Johnson, F. (2006) Synthesis of the PhIP adduct of 2′-deoxyguanosine and its incorporation into oligomeric DNA. *Chem. Res. Toxicol. 19*, 734–738.

(29) Patel, D. J., Mao, B., Gu, Z., Hingerty, B. E., Gorin, A., Basu, A. K., and Broyde, S. (1998) Nuclear magnetic resonance solution structures of covalent aromatic amine-DNA adducts and their mutagenic relevance. *Chem. Res. Toxicol. 11*, 391–407.

(30) Patnaik, S., and Cho, B. P. (2010) Structures of 2-acetylaminofluorene modified DNA revisited: Insight into conformational heterogeneity. *Chem. Res. Toxicol. 23*, 1650–1652.

(31) O'Handley, S. F., Sanford, D. G., Xu, R., Lester, C. C., Hingerty, B. E., Broyde, S., and Krugh, T. R. (1993) Structural characterization of an N-acetyl-2-aminofluorene (AAF) modified DNA oligomer by NMR, energy minimization, and molecular dynamics. *Biochemistry 32*, 2481–2497.

(32) Omumi, A., Beach, D. G., Baker, M., Gabryelski, W., and Manderville, R. A. (2011) Post-synthetic guanine arylation of DNA by Suzuki-Miyaura cross-coupling. *J. Am. Chem. Soc. 133*, 42–50.

(33) Schlitt, K. M., Sun, K. M., Paugh, R. J., Millen, A. L., Navarro-Whyte, L., Wetmore, S. D., and Manderville, R. A. (2009) Concerning the hydrolytic stability of 8-aryl-2′-deoxyguanosine nucleoside adducts: Implications for abasic site formation at physiological pH. *J. Org. Chem. 74*, 5793–5802.

(34) Weishar, J. L., McLaughlin, C. K., Baker, M., Gabryelski, W., and Manderville, R. A. (2008) Oxidation of a biomarker for phenol carcinogen exposure: Expanding the redox chemistry of 2′-deoxyguanosine. *Org. Lett. 10*, 1839–1842.

(35) Cahová, H., Pohl, R., Bednárová, L., Nováková, K., Cvăcka, J., and Hocek, M. (2008) Synthesis of 8-bromo-, 8-methyl- and 8-phenyl-dATP and their polymerase incorporation into DNA. *Org. Biomol. Chem. 6*, 3657–3660.

(36) McLaughlin, C. K., Lantero, D. R., and Manderville, R. A. (2006) Conformational properties of a phototautomerizable nucleoside biomarker for phenolic carcinogen exposure. *J. Phys. Chem. A 110*, 6224–6230.

(37) Sun, K. M., McLaughlin, C. K., Lantero, D. R., and Manderville, R. A. (2007) Biomarkers for phenol carcinogen exposure act as pH-sensing fluorescent probes. *J. Am. Chem. Soc. 129*, 1894–1895.

(38) Millen, A. L., McLaughlin, C. K., Sun, K. M., Manderville, R. A., and Wetmore, S. D. (2008) Computational and experimental evidence for the structural preference of phenolic C-8 purine adducts. *J. Phys. Chem. A 112*, 3742–3753.

(39) Geacintov, N. E., Cosman, M., Mao, B., Alfano, A., Ibanez, V., and Harvey, R. G. (1991) Spectroscopic characteristics and site I/site II classification of cis and trans benzo[a]pyrene diolepoxide enantiomer-guanosine adducts in oligonucleotides and polynucleotides. *Carcinogenesis 12*, 2099–2108.

(40) Nolan, S. J., Vyas, R. R., Hingerty, B. E., Ellis, S., Broyde, S., Shapiro, R., and Basu, A. K. (1996) Solution properties and computational analysis of an oligodeoxynucleotide containing N-(deoxyguanosin-8-yl)-1-aminopyrene. *Carcinogenesis 17*, 133–144.

(41) Millen, A. L., Manderville, R. A., and Wetmore, S. D. (2010) Conformational flexibility of C8-phenoxyl-2′-deoxyguanosine nucleotide adducts (2010). *J. Phys. Chem. B 114*, 4373–4382.

(42) Millen, A. L., Churchill, C. D. M., Manderville, R. A., and Wetmore, S. D. (2010) Effect of Watson-Crick and Hoogsteen base pairing on the conformational stability of C8-phenoxyl-2′-deoxyguanosine adducts. *J. Phys. Chem. B 114*, 12995–13004.

(43) Gillet, L., and Schärer, O. D. (2002) Preparation of C8-amine and acetylamine adducts of 2′-deoxyguanosine suitably protected for DNA synthesis. *Org. Lett. 4*, 4205–4208.

(44) Western, E. C., Daft, J. R., Johnson, E. M., II, Gannett, P. M., and Shaughnessy, K. H. (2003) Efficient one-step Suzuki arylation of unprotected halonucleosides, using water-soluble palladium catalysts. *J. Org. Chem. 68*, 6767–6774.

(45) Fery-Forgues, S., and Lavabre, D. (1999) Are fluorescence quantum yields so tricky to measure? A demonstration using familiar stationery products. *J. Chem. Educ. 76*, 1260–1264.

(46) Demas, J. N., and Crosby, G. A. (1971) The measurement of photoluminescence quantum yields. *J. Phys. Chem. 75*, 991–1024.

(47) Peréz, A., Marchán, I., Svozil, D., Sponer, J., Cheatham, T. E., III, Laughton, C. A., and Orozco, M. (2007) Refinement of the AMBER force field for nucleic acids: Improving the description of α/γ conformers. *Biophys. J. 92*, 3817–3829.

(48) Heavner, S., and Gannett, P. M. (2005) Molecular dynamics and free energy calculations of the B and Z forms of C8-arylguanine modified oligonucleotides. *J. Biomol. Struct. Dyn. 23*, 203–219.

(49) Wang, J., Wang, W., Kollman, P. A., and Case, D. A. (2006) Automatic atom type and bond type perception in molecular mechanical calculations. *J. Mol. Graphics Modell. 25*, 247–260.

(50) Dupradeau, F.-Y., Pigache, A., Zaffran, T., Savineau, C., Lelong, R., Grivel, N., Lelong, D., Rosanski, W., and Cieplak, P. (2010) The R.E.D. tools: Advances in RESP and ESP charge derivation and force field library building. *Phys. Chem. Chem. Phys. 12*, 7821–7839.

(51) Pigache, A.; Cieplak, P.; Dupradeau, F.-Y. Automatic and highly reproducible RESP and ESP charge derivation: Application to the development of programs R.E.D. and X R.E.D, 227th ACS National Meeting, Anaheim, CA, March 28−April 1, 2004.

(52) Cheatham, T. E., III, Cieplak, P., and Kollman, P. A. (1999) Molecular dynamics simulations of nucleic acids. *J. Biomol. Struct. Dyn. 16*, 845–862.

(53) Frisch, M. J., Trucks, G. W., Schlegel, H. B., Scuseria, G. E., Robb, M. A., Cheeseman, J. R., Montgomery, J. A., Jr., Vreven, T., Kudin, K. N., Burant, J. C., Millam, J. M., Iyengar, S. S., Tomasi, J., Barone, V., Mennucci, B., Cossi, M., Scalmani, G., Rega, N., Petersson, G. A., Nakatsuji, H., Hada, M., Ehara, M., Toyota, K., Fukuda, R., Hasegawa, J., Ishida, M., Nakajima, T., Honda, Y., Kitao, O., Nakai, H., Klene, M., Li, X., Knox, J. E., Hratchian, H. P., Cross, J. B., Bakken, V., Adamo, C., Jaramillo, J., Gomperts, R., Stratmann, R. E., Yazyev, O., Austin, A. J., Cammi, R., Pomelli, C., Ochterski, J. W., Ayala, P. Y., Morokuma, K., Voth, G. A., Salvador, P., Dannenberg, J. J., Zakrzewski, V. G., Dapprich, S., Daniels, A. D., Strain, M. C., Farkas, O., Malick, D. K., Rabuck, A. D., Raghavachari, K., Foresman, J. B., Ortiz, J. V., Cui, Q., Baboul, A. G., Clifford, S., Cioslowski, J., Stefanov, B. B., Liu, G., Liashenko, A., Piskorz, P., Komaromi, I., Martin, R. L., Fox, D. J., Keith, T., Al-Laham, M. A., Peng, C. Y., Nanayakkara, A., Challacombe, M., Gill, P. M. W., Johnson, B., Chen, W., Wong, M. W., Gonzalez, C., and Pople, J. A. (2003) *Gaussian 03*, revision D.02, Gaussian, Inc., Wallingford, CT.

(54) Case, D. A., Darden, T. A., Cheatham, T. E., III, Simmerling, C. L., Wang, J., Duke, R. E., Luo, R., Crowley, M., Walker, R. C., Zhang, W., Merz, K. M., Wang, B., Hayik, S., Roitberg, A., Seabra, G., Kolossváry, I., Wong, K. F., Paesani, F., Vanicek, J., Wu, X., Brozell, S. R., Steinbrecher, T., Gohlke, H., Yang, L., Tan, C., Mongan, J., Hornak, V., Cui, G., Mathews, D. H., Seetin, M. G., Sagui, C., Babin, V., and Kollman, P. A. (2008) *AMBER 10*, University of California, San Francisco.

(55) Case, D. A., Darden, T. A., Cheatham, T. E., III, Simmerling, C. L., Wang, J., Duke, R. E., Luo, R., Walker, R. C., Zhang, W., Merz, K. M., Roberts, B. P., Wang, B., Hayik, S., Roitberg, A., Seabra, G., Kolossváry, I., Wong, K. F., Paesani, F., Vanicek, J., Liu, J., Wu, X., Brozell, S. R., Steinbrecher, T., Gohlke, H., Cai, Q., Ye, X., Wang, J., Hsieh, M.-J., Cui, G., Roe, D. R., Mathews, D. H., Seetin, M. G., Sagui, C., Babin, V., Luchko, T., Gusarov, S., Kovalenko, A., and Kollman, P. A. (2010) *AMBER 11*, University of California, San Francisco, CA.

(56) Dennington, R., Keith, T., and Millam, J. *GaussView*, Version 5 (2009) Semichem Inc., Shawnee Mission, KS.

(57) Jorgensen, W. L., Chandrasekhar, J., Madura, J. D., Impey, R. W., and Klein, M. L. (1983) Comparison of simple potential functions for simulating liquid water. *Chem. Phys. 79*, 926–935.

(58) Essmann, U., Perera, L., Berkowitz, M. L., Darden, T., Lee, H., and Pedersen, L. G. (1995) A smooth particle mesh Ewald method. *J. Chem. Phys. 103*, 8577–8593.

(59) Ryckaert, J. P., Ciccotti, G., and Berendsen, H. J. C. (1977) Numerical Integration of the Cartesian Equations of Motion of a System with Constraints: Molecular Dynamics of n-Alkanes. *J. Comput. Phys. 23*, 327–341.

(60) Zhao, Y., and Truhlar, D. G. (2008) The M06 suite of density functionals for main group thermochemistry, thermochemical kinetics, noncovalent interactions, excited states, and transition elements: Two new functionals and systematic testing of four M06-class functionals and 12 other functional. *Theor. Chem. Acc. 120*, 215–241.

(61) Frisch, M. J., Trucks, G. W., Schlegel, H. B., Scuseria, G. E., Robb, M. A., Cheeseman, J. R., Scalmani, G., Barone, V., Mennucci, B., Petersson, G. A., Nakatsuji, H., Caricato, M., Li, X., Hratchian, H. P., Izmaylov, A. F., Bloino, J., Zheng, G., Sonnenberg, J. L., Hada, M., Ehara, M., Toyota, K., Fukuda, R., Hasegawa, J., Ishida, M., Nakajima, T., Honda, Y., Kitao, O., Nakai, H., Vreven, T., Montgomery, J. A., Jr., Peralta, J. E., Ogliaro, F., Bearpark, M., Heyd, J. J., Brothers, E., Kudin, K. N., Staroverov, V. N., Kobayashi, R., Normand, J., Raghavachari, K., Rendell, A., Burant, J. C., Iyengar, S. S., Tomasi, J., Cossi, M., Rega, N., Millam, J. M., Klene, M., Knox, J. E., Cross, J. B., Bakken, V., Adamo, C., Jaramillo, J., Gomperts, R., Stratmann, R. E., Yazyev, O., Austin, A. J., Cammi, R., Pomelli, C., Ochterski, J. W., Martin, R. L., Morokuma, K., Zakrzewski, V. G., Voth, G. A., Salvador, P., Dannenberg, J. J., Dapprich, S., Daniels, A. D., Farkas, O., Foresman, J. B., Ortiz, J. V., Cioslowski, J., and Fox, D. J. (2009) *Gaussian 09*, revision A.02, Gaussian, Inc., Wallingford, CT.

(62) Siriwong, K., Voityuk, A. A., Newton, M. D., and Rösch, N. (2003) Estimate of the reorganization energy for charge transfer in DNA. *J. Phys. Chem. B 107*, 2595–2601.

(63) Schwalb, N. K., Michalak, and Temps, F. J. (2009) Ultrashort fluorescence lifetimes of hydrogen-bonded base pairs of guanosine and cytidine in solution. *J. Phys. Chem. B 113*, 16365–16376.

(64) Onidas, D., Markovitsi, D., Marguet, S., Sharonov, A., and Gustavsson, T. (2002) Fluorescence properties of DNA nucleosides and nucleotides: A refined steady-state and femtosecond investigation. *J. Phys. Chem. B 106*, 11367–11374.

(65) Jamison, J. L., Davenport, L., and Williams, B. W. (2006) Solvatochromism in the aromatic ketone benzo[b]fluorenone. *Chem. Phys. Lett. 422*, 30–35.

(66) Gray, D. M., Liu, Ratliff, R. L., and Vaughan, M. R. (1992) Circular dichroism spectroscopy of DNA. *Methods Enzymol. 211*, 389–406.

(67) McConnell, T. L., and Wetmore, S. D. (2007) How do size-expanded DNA nucleobases enhance duplex stability? Computational analysis of the hydrogen-bonding and stacking ability of xDNA bases. *J. Phys. Chem. B 111*, 2999–3009.

(68) Kelly, R. E. A., Lee, Y. J., and Kantorovich, L. N. (2005) Homopairing Possibilities of the DNA Bases Cytosine and Guanine: An ab Initio DFT Study. *J. Phys. Chem. B 109*, 22045–22052.

(69) Jurecka, P., and Hobza, P. (2003) True stabilization energies for the optimal planar hydrogen-bonded and stacked structures of guanine···cytosine, adenine···thymine, and their 9-and 1-methyl derivatives: Complete basis set calculations at the MP2 and CCSD(T) levels and comparison with experiment. *J. Am. Chem. Soc. 125*, 15608–15613.

(70) Kabelac, M., and Hobza, P. (2001) Potential energy and free energy surfaces of all ten canonical and methylated nucleic acid base pairs: Molecular dynamics and quantum chemical ab initio studies. *J. Phys. Chem. B 105*, 5804–5817.

(71) Sponer, J., Leszczynski, J., and Hobza, P. (2001) Electronic properties, hydrogen bonding, stacking, and cation binding of DNA and RNA bases. *Biopolymers 61*, 3–31.

(72) Valis, L., Mayer-Enthart, E., and Wagenknecht, H.-A. (2006) 8-(Pyren-1-yl)-2′-deoxyguanosine as an optical probe for DNA hybridization and for charge transfer with small peptides. *Bioorg. Med. Chem. Lett. 16*, 3184–3187.

(73) Elmquist, C. E., Wang, F., Stover, J. S., Stone, M. P., and Rizzo, C. J. (2007) Conformational differences of the C8-deoxyguanosine adduct of 2-amino-3-methylimidazo[4,5-f]quinolone (IQ) within the NarI recognition sequence. *Chem. Res. Toxicol. 20*, 445–454.

(74) Koehl, P., Valladier, P., Lefevre, J. F., and Fuchs, R. P. P. (1989) Strong structural effect of the position of a single acetylaminofluorene within a mutation hot spot. *Nucleic Acids Res. 17*, 9531–9541.

(75) Simonsson, T. (2001) G-Quadruplex DNA structures—Variations on a theme. *Biol. Chem. 382*, 621–628.

(76) Esposito, V., Randazzo, A., Piccialli, G., Petraccone, L., Giancola, C., and Mayol, L. (2004) Effects of an 8-bromodeoxyguanosine incorporation on the parallel quadruplex structure $[d(TGGGT)]_4$. *Org. Biomol. Chem. 2*, 313–318.

(77) Dumas, A., and Luedtke, N. W. (2010) Cation-mediated energy transfer in G-quadruplexes revealed by an internal fluorescent probe. *J. Am. Chem. Soc. 132*, 18004–18007.

(78) Dupradeau, F.-Y., Case, D. A., Yu, C., Jimenez, R., and Romesberg, F. E. (2005) Differential solvation and tautomer stability of a model base pair within the minor and major grooves of DNA. *J. Am. Chem. Soc. 127*, 15612–15617.

(79) Kohda, K., Tsunomoto, H., Kasamatsu, T., Sawamura, F., Terashima, I., and Shibutani, S. (1997) Synthesis and miscoding specificity of oligonucleotide containing 8-phenyl-2′-deoxyguanosine. *Chem. Res. Toxicol. 10*, 1351–1358.